Ana de Souto Martins
Licenciatura em Genética e Biotecnologia

Interaction of West-Nile virus capsid protein with lipid systems

Dissertação para obtenção do Grau de Mestre em
Genética Molecular e Biomedicina

Orientador: Nuno C. Santos, Professor Doutor, IMM
Co-orientador: Ivo C. Martins, Doutor, IMM

Júri:

Presidente: Prof. Doutora Ilda Maria Barros dos Santos Gomes Sanches
Arguente: Prof. Doutor José Ricardo Ramos Franco Tavares
Vogal: Prof. Doutor Nuno Fernando Duarte Cordeiro Correia dos Santos

FACULDADE DE CIÊNCIAS E TECNOLOGIA
UNIVERSIDADE NOVA DE LISBOA

Outubro 2014

Ana de Souto Martins
Licenciatura em Genética e Biotecnologia

Interaction of West-Nile virus capsid protein with lipid systems

Dissertação para obtenção do Grau de Mestre em
Genética Molecular e Biomedicina

Orientador: Nuno C. Santos, Professor Doutor, IMM
Co-orientador: Ivo C. Martins, Doutor, IMM

Júri:

Presidente: Prof. Doutora Ilda Maria Barros dos Santos Gomes Sanches
Arguente: Prof. Doutor José Ricardo Ramos Franco Tavares
Vogal: Prof. Doutor Nuno Fernando Duarte Cordeiro Correia dos Santos

FACULDADE DE CIÊNCIAS E TECNOLOGIA
UNIVERSIDADE NOVA DE LISBOA

Outubro 2014

Interaction of West-Nile virus capsid protein with lipid systems

Acknowledgments

I want to thank and express my gratitude to everyone of the N.Santos lab of the IMM. All members, in some way, helped me to develop this work. To Prof. Nuno C. Santos, Head of the Unit and my supervisor, I owe all my gratitude for having provided me all the conditions I need and the excellent accompaniment at every moment. He encouraged me to continue and not giving up. I am also grateful to Dr. Ivo C. Martins, co-supervisor of my thesis, who constantly accompanied me in the laboratory work as well as in all steps of my thesis. I am especially thankful to Filomena A. Carvalho that also supported me and shared with me several crucial techniques for this project. She is an excellent professional who provides her time to teach all the processes in detail. I owe a special thanks to André F. Faustino who helped me to integrate many techniques and in crucial moments he always had time to teach me. To Teresa Freitas that supported me with technical assistance and helped me with some processes in the lab, I thank all this and their affection, comprehension and good humor every day. Also, there are various persons that we call the “the youngers” that made me very happy to have been part of this group (they are wonderful people with whom I enjoyed working). I can say that, Susana Reis was part of my whole journey in IMM, in the good and the less good moments she always had something to tell me and back me up.

To my friends from Vila Real, who shared with me the best moments of academic life and were always present despite the distance I thank you for reached with me this stage of my life. A special thanks to Diana, Ana, Ângela, Cátia, M. João and Soraia.

To my old friends from Almada, I do not even have words, they are part of a big and wonderful second family that will be to last a lifetime. They are really friends forever and for everything.

I want to acknowledge my family for always having being by my side. They were patient with me in all bad moments and with much sacrifice supported me. With my mother, my best friend, I learned not to give up and always fight for what I think it is right. My older brothers, Jorge and Luis, were my real support, my pride and forever an example to follow. They really battled for helping me to achieve everything I have today. I have a final word for the newest member of the family “the little”, who certainly will accomplish me in the future.

I dedicate this thesis to my older twin brothers.
They are not only brothers, they are everything to me.

Abstract

West-Nile Virus (WNV) infection occurs through the bite of *Culex* spp. mosquitoes and constitutes a serious public health threat. Despite the global spread and disease severity, there is no specific and effective treatment for WNV infection, in part due to a poor understanding of the virus life cycle. A key viral life cycle step is viral assembly and encapsidation, mediated by the capsid (C) protein interaction with RNA and host lipid structures. WNV C interactions with intracellular lipid droplets (LDs) and with very low-density lipoproteins (VLDL), crucial step for successful viral replication in related members of the *Flaviviridae* family, were studied via biophysical approaches. Zeta potential measurements showed that WNV C interaction with LDs requires K^+ and LDs surface proteins. WNV C interaction with lipoproteins measured via dynamic light scattering (DLS), showed that WNV C binds to VLDL but not to low-density lipoproteins (LDL), in a potassium dependent manner. It was clear that in the presence of WNV C there is an increase of the VLDL hydrodynamic radius that correlates very well with WNV C estimated dimension. The WNV C (un)binding forces upon interaction with LDs and VLDL were quantitatively determined by atomic force microscopy (AFM)-based force spectroscopy. WNV C specifically binds to LDs and VLDL, in a potassium-dependent manner, but not to LDL. DLS was also performed to determine pep14-23 (an inhibitor of dengue virus – DENV – C protein interaction with LDs and VLDL) effect on WNV C-VLDL binding. Data obtained indicate that pep14-23 may also be a potential inhibitor for WNV C key interactions. The results obtained in this study are in agreement with the previously observed for DENV, showing that WNV C and DENV C proteins interact in a similar manner with LDs and VLDL, and suggesting pep14-23 as a potential inhibitor of *Flavivirus* C proteins binding to host lipid systems.

Keywords: West-Nile virus; capsid protein; lipid droplets; lipoproteins; pep14-23.

Resumo

A infeção com o Vírus do Nilo Ocidental (WNV *do inglês*) ocorre atrvavés da picada de mosquitos *Culex* spp. e constitui uma séria ameaça para a saúde pública. Apesar da sua disseminação a nível mundial e da severidade da doença, não existe um tratamento específico e eficaz, devido (em parte) à necessidade de um melhor conhecimento do ciclo de vida do vírus. Um passo chave do ciclo de vida viral é a montagem e a encapsidação do virus, mediada pela interação da proteína da cápside (C) com RNA viral e estruturas lipídicas do hospedeiro. A interação da WNV C com corpúsculos lipídicos (LDs *do inglês*) intracelulares e com lipoproteínas de muito baixa densidade (VLDL *do inglês*), um passo crucial para o sucesso da replicação viral em membros relacionados da família *Flaviviridae,* foi estudada através de técnicas biofísicas. As medidas de potencial zeta mostraram que a interação da WNV C com LDs requer K^+ e poteínas à superfície das LDs. A interação da WNV C com liporpteínas medida por dispersão dinâmica de luz (DLS *do inglês*), mostrou que a WNV C liga-se às VLDL mas não às lipoproteínas de baixa densidade (LDL *do inglês*), numa interação dependente de potássio. Foi evidente que na presença de WNV C existe um aumento do raio hidrodinâmico das VLDL que se correlaciona muito bem com as dimesões estimadas para a WNV C. As forças de ligação da WNV C com LDs e VLDL foram quantificadas por espectroscopia de força baseada em microscopia de força atómia (AFM). A WNV C liga-se especificamente às LDs e às VLDL, numa interação dependente de potássio, mas não às LDL. A DLS também foi realizada para determinar o efeito do pep14-23 (um inibidor da interação da proteína C do vírus da dengue – DENV *do inglês* – com LDs e VLDL) na ligação WNV C-VLDL. Os dados obtidos indicam que o pep14-23 também poderá ser um potencial inibidor das interações chave da WNV C. Os resultados obtidos neste estudo estão de acordo com os observados previamente para o DENV, mostrando que a WNV C e a DENV C interagem de uma maneira semelhante com as LDs e as VLDL, e sugerem o pep14-23 como um potencial inibidor da ligação das proteínas C de *Flavivirus* com sistemas lipídicos do hospedeiro.

Palavras-chave: Vírus do Nilo Ocidental; proteína da cápside; corpúsculos lipídicos; lipoproteínas; pep14-23.

Contents

Acknowledgments ... **iii**

Abstract ... **v**

Resumo ... **vii**

Index of Figures ... **xi**

Index of Tables ... xv

Abbreviations and Symbols ... **xvii**

I - Introduction ... **1**

West-Nile virus epidemics and global impact ... **2**

Spread and mode of transmission ... **2**

Symptoms and diagnosis ... **4**

West-Nile virus life cycle and structure ... **6**

Viral life cycle ... **6**

The virus structure ... **7**

The capsid protein ... **8**

Lipid droplets and lipoproteins in *Flaviviridae* infections ... **9**

Lipid droplets ... **9**

Plasma lipoproteins ... **11**

Rationale for the study of WNV C protein interaction with lipid systems ... **13**

Aims and Goals ... **16**

II - Methodology ... **17**

Biophysical approaches ... **18**

Dynamic light scattering ... **18**

Zeta Potential ... **20**

Atomic force microscopy-based force spectroscopy ... **21**

Material & Methods ... **24**

Materials ... **24**

Cell culture and lipid droplets isolation ... **24**

Lipid droplets purification ... **25**

ζ-potential analysis of LDs surface charge ... **25**

LDs and lipoproteins preparation for force spectroscopy measurements ... **26**

Functionalization of AFM tips with WNV C ... **26**
AFM-based force spectroscopy measurements ... **26**
DLS measurements of lipoproteins ... **27**
III - WNV C interaction with Lipid Droplets ... **29**
Background ... **30**
Results ... **32**
Assessment of WNV C protein-LDs interaction by ζ-potential analysis ... **32**
Assessment of WNV C-LDs interaction by AFM-based force spectroscopy ... **34**
Discussion ... **37**
IV - WNV C interaction with Lipoproteins ... **39**
Background ... **40**
Results ... **42**
Assessment of WNV C-VLDL interaction by dynamic light scattering ... **42**
Assessment of WNV C-VLDL interaction by AFM-based force spectroscopy ... **44**
pep14-23, a possible inhibitor of WNVC-VLDL interaction ... **46**
Discussion ... 48
V - General Conclusions ... **51**
Future Work ... **53**
References ... **55**
Annexes ... **61**

Index of Figures

Figure 1.1 - Global distribution of *Cx. pipiens* complex mosquitoes. Geographic range for *Cx. p. pipiens* includes both forms (*pipiens* and *molestus*). *Cx. australicus* and *Cx. globocoxitus* are restricted to Australia (Ciota and Kramer, 2013). **2**

Figure 1.2 - **European distribution of West Nile Virus.** Sporadic cases of disease in horses and humans were observed occasionally in France, Portugal, Spain, Italy, Czech Republic, Romania, and Hungary (Pauli *et al*., 2013). **4**

Figure 1.3 - *Flavivirus* life cycle. *Flavivirus* enter in the host cell by receptor-mediated endocytosis. Acidification of the endosomal vesicle conduct to the fusion of the viral and cell membranes and the genome ss(+)RNA is released into the cytoplasm. The ss(+)RNA is translated in a polyprotein that is processed by viral and host proteases, originating seven non-structural proteins and three structural proteins. Non-structural proteins promote the viral genome replication near the ER and structural proteins are involved in the viral assembly in the surface of the ER. After the virion maturation by the host protease furin, the mature virion follows the secretion pathway and subsequently is released by exocytosis (Mukhopadhyay *et al.*, 2005). **7**

Figure 1.4 - Structures of dengue and West-Nile viruses determined by cryo-electron microscopy. (A) Cryo-EM image of a DENV particle. (B) Cryo-EM image of a WNV particle. Virion cores contain the nucleocapsid, where the viral genomic RNA is conjugated with multiple C protein copies; surrounded the nucleocapsid is a lipid bilayer derived from the host cell ER; the outer layer envelope is constituted by the E protein that is capped by the prM protein before maturation (Mukopadhyay *et al*., 2003; Yu *et al*., 2008) **8**

Figure 1.5 - Dimer structure of *Flavivirus* C proteins. The four α helices (α1 to α4) are indicated in each monomer. C proteins form an α-helical homodimer with an asymmetric charge distribution. The α2-α2' interface, highly hydrophobic, interacts with membranes and the α4-α4' region, mainly positively-charged, interacts with RNA. Adapted from Samsa *et al.*, 2009. ..... **9**

Figure 1.6 - LDs structure. LDs form at the ER, where the enzymes that catalyze neutral lipid synthesis are located. LDs structure comprises a neutral lipid core surrounded by a phospholipid monolayer that harbors small amounts of free cholesterol. Multiple proteins interact with the LDs surface through different structural features. The main LDs proteins are perilipin, ADRP and TIP47 (from the PAT family) (Krahmer *et al*., 2009). **10**

Figure 1.7 - Interaction of DENV C protein with LDs is required for DENV C replication. (A) Image of confocal microscopy: the C protein is targeted to LDs. DENV infected cells accumulate the C protein around LDs. (B) Effect of C75, an inhibitor of LDs formation, on the amount of LDs in BHK cells. The number of LDs decrease in cells infected and non-infected with DENV. (C) Viral replication was also inhibited. Adapted from Samsa *et al*., 2009. ..... **11**

Figure 1.8 - Sequence and structural similarity between apoE N-terminus and perilipin 3 C-terminus. (A) Sequences of apoE N-terminus (first 220 residues) and perilipin 3 C-terminus (last 220 residues) show several similar regions, which could be involved in similar functions/interactions. Equal residues present in both of the aligned sequences (red); stereochemically and/or functionally identical residues (black). In the sequence consensus, "h", "+" and "−" stand respectively for hydrophobic, positively-charged and negatively-charged residues at the same aligned position. (B) The structures of apoE N-terminus (PDB ID: 2KC3 [red]) and perilipin 3 C-terminus (PDB ID: 1SZI [green]) superimpose in space through its common four-helix-bundle motif. Adapted from Faustino *et al.*, 2014. ..... **13**

Figure 1.9 - C protein residues involved in the LD interaction are conserved among *Flavivirus* spp. (A) Alignment of the DENV C protein sequence with C protein sequences from other flaviviruses, highlighting fully conserved segments (red) and partially conserved residues (black). (B) Comparison of C protein structures of DENV (grey) and WNV-K (red). Two regions can be depicted: a conserved fold (from residues 44 to the C-terminus), and a particularly flexible region with alternative folds, containing α1 and the disordered section (residues 1–26). Adapted from Martins *et al*., 2012..... **15**

Figure 2.1 - Dynamic light scattering principle. (A) Particle size can be determined through the measurement of the scattering light intensity fluctuations as a function of the time *I* (t). Each intensity value is correlated with the others, through autocorrelation functions (*CC*(*t*) is the correlation coefficient of the *I*(*t*) function). Larger particles generate higher correlation than smaller ones, because their motion is slower. Through the autocorrelation function and the Stokes-Einstein equation, D_H can be determined. (B) The intensity function of D_H can be transformed in the particle number distribution of D_H. **20**

Figure 2.2 - ζ-potential of a particle: distribution of counterions in the double layer surrounding a negatively charged particle. The ζ-potential of a particle is proportional to its surface charge. The particle negatively charged in suspension attracts counterions of the solution to their surface, which forms the Stern layer. This layer of counterions is depicted as tightly bound to the charged particle surface. The electric potential between the second layer boundary of the shear plane and the solution is the ζ-potential. When an electric field, which changes the polarity with a given frequency, is applied to the solution, the particles move and the phase shift in the scattered beam is measured along time (Uskoković, 2012). **21**

Figure 2.3 - Components of an atomic force microscope and different tip (or sample) movements. (A) AFM technique is based on the force applied by a nanometer-sharped tip, which can be functionalized, on the sample surface. A laser is reflected on the cantilever surface and its deflection can be measured with a photodiode detector. To scan the surface, the tip can do two different movements, (B) drag across the surface to a contact mode imaging or (C) vibrate as it moves along the surface to an intermittent contact mode imaging. In some equipments, to achieve these types of imaging, it is the sample holder that moves, while the tip remains on the same position (Whited and Park, 2014)..... **22**

Figure 2.4 - AFM-based force microscopy. (A) Schematic diagram of a typical force-distance measurement cycle. With a protein functionalized tip (a tip functionalized with WNV C in this case), performing approach and retraction cycles on the sample (LDs and plasma lipoproteins in the present study), the force and distance necessary for the unbinding event are measured. When no interactions are observed, a curve as in the top of panel B is generated; if the protein binds to the sample surface, a curve as in the bottom of panel B is generated. With the information from hundreds or thousands of these curves, the histograms (C) are generated, in order to calculate the interaction parameters. **23**

Figure 3.1 - LDs zeta potential analysis with DENV C protein. (A) LDs zeta potential values determined in the absence and in the presence of distinct DENV C concentrations, at different KCl concentrations. (B) Values of the maximum amplitude of variation of the LDs zeta potential ($\Delta\zeta_{max}$) induced by the interaction with the DENV C protein and DENV C protein concentration at $\Delta\zeta_{max}/2$ ($C_{1/2}$) in TEE buffer with different potassium concentrations (Carvalho *et al.,* 2012). **31**

Figure 3.2 - LDs ζ-potential analysis at different WNV C concentrations. Variation of zeta potential ($\Delta\zeta$) values of LDs samples isolated with (A) TEE-KCl buffer (K^+ buffer) and (B) TEE-NaCl buffer (Na^+ buffer) in the absence and in the presence of distinct WNV C concentrations. ζ-potential values were determined for LDs without trypsin preincubation (filled symbols) and LDs preincubated with trypsin (empty symbols). Results are represented as mean ± standard error. Solid lines were obtained

through the fitting of experimental data with equation 10. Concentrations are presented in logarithmic scale. **33**

Figure 3.3 - Force rupture histograms of the binding of WNV C to BHK-21 LDs in TEE buffer with (A) 100 mM KCl and (B) 10 mM KCl. Four peaks of rupture forces were observed for TEE buffer with 100 mM KCl (1: 17.67 ± 47.81 pN; 2: 30.38 ± 0.33 pN; 3: 52.04 ± 2.49 pN; 4: 108.52 ± 2.82 pN) and two peaks for TEE buffer with 10 mM KCl (1: 20.05 ± 0.19 pN; 2: 29.59 ± 0.89 pN). **35**

Figure 3.4 - Force rupture histogram of the binding of WNV C to BHK-21 LDs in TEE buffer with 100 mM NaCl. One peak of rupture force at 17.88 ± 0.14 pN was observed between WNV C and LDs in TEE buffer with 100 mM NaCl. **36**

Figure 4.1 - Lipoproteins average diameter evolution upon titration with DENV C determined by DLS. DENV C interacts with VLDL (red) and forms a conjugate with a D_H ~6 nm higher than in the absence of DENV C (*p < 0.005). LDL (blue) do not form the same type of conjugate (no statistically significant variations on D_H (p > 0.05), indicating that DENV C does not interact with LDL (Faustino *et al.*, 2014)..... **40**

Figure 4.2 - DLS analysis of lipoproteins in potassium buffer. Lipoproteins hydrodynamic diameters (D_H) were determined in the absence and in the presence of increasing WNV C concentrations. VLDL (blue) average hydrodynamic diameter increases in the presence of WNV C, ΔD_H = 4.5 ± 0.6 nm. The D_H of LDL (green) in the absence and presence of WNV C do not change significantly, only with higher concentration of WNV C (5µM) a statistically significant variation (p < 0.005) occurs. The values represented are the average of all measurements for each point (error bars represent standard error and dashed lines the average of each set of points)..... **42**

Figure 4.3 - DLS analysis of VLDL in sodium buffer. VLDL hydrodynamic diameters (D_H) were determined in the absence and in the presence of increasing WNV C concentrations in TEE NaCl 100 mM buffer. The D_H of VLDL in the absence and presence of WNV C do not change significantly. The values represented are the average of all measurements for each point. Error bars represent standard error and the dashed line the average of all points. **43**

Figure 4.4 - Model for the interaction of WNV C with VLDL. The dimensions of WNV C fit well with the observed increase of ~4.5 nm on the VLDL hydrodynamic diameter (~2.3 nm for the radius), determined by DLS. In the absence of WNV C, VLDL presented a radius of ~19 nm. In the presence of WNV C 5 µM, VLDL presented a radius of ~21.3 nm. WNV C seems to bind to the VLDL surface in a sufficient number to cause a significant increase on their size, forming a protein monolayer. This monolayer does not have to be continuous..... **44**

Figure 4.5 - Force rupture histograms of WNV C interactions with (A) VLDL or (B) LDL, in TEE buffer with 100 mM KCl. Two rupture force peaks were observed for VLDL (1: 20.96 ± 0.29 pN; 2: 82.88 ± 0.65 pN) and one for LDL (24.53 ± 0.09 pN)..... **45**

Figure 4.6 - Force rupture histogram of WNV C interaction with VLDL in TEE buffer with 100 mM NaCl. Only one rupture force peak is observed (24.96 ± 0.08 pN). **46**

Figure 4.7 - DLS correlograms of 50-fold diluted VLDL measured in different conditions: blue line – VLDL alone; red line – VLDL incubated with pep14-23 100µM; green line – VLDL preincubated with pep14-23 100µM and after with WNV C 5 µM; black line – VLDL and WNV C..... **47**

Index of Tables

Table 1.1 - LDL, VLDL, LDs and LVP structure composition. The structure of all these systems is similar: a core of neutral lipids is surrounded by a monolayer of polar lipids where specific proteins are embedded. Their different lipid composition give them a different density. VLDL are very similar to LDs and lipoviroparticles (LVPs) in terms of lipid composition (Faustino *et al*., 2014). **12**

Table 3.1 - Rupture forces and percentage of (un)binding events obtained for interactions between DENV C and LDs obtained from HepG2 cell line, under diverse experimental conditions. The percentage of (un)binding events and the rupture force decrease with the reduction of potassium concentration, as well as with trypsin treatments and the replacement of potassium by sodium ions (Carvalho *et al.,* 2012). **30**

Table 3.2 - Parameters obtained by ζ-potential analysis of LDs under different conditions. The values of $C_{1/2}$ and $\Delta\zeta_{max}$ were obtained through the fitting of ζ-potential experimental data with equation 10. ..... **33**

Table 3.3 - Rupture forces and percentage of (un)binding events observed with AFM-based force spectroscopy for the interaction between WNV C and BKH-21 LDs at different experimental conditions. **36**

Table 4.1 - Rupture forces and percentage of (un)binding events determined with AFM-based force spectroscopy for the interaction between WNV C and VLDL or LDL at different experimental conditions. **46**

Abbreviations and Symbols

ADRP – adipose differentiation-related protein or perilipin 2, an LDs protein

AFM – atomic force microscopy

apo – apolipoprotein or apoprotein

apoB100, C-I, C-II, C-III, E – apolipoproteins from VLDL (apoB100 is almost the unique protein present in LDL)

APTES – 3-aminopropyl-triethoxysilane

BBB – blood-brain barrier

BHK/ BHK-21 – baby hamster kidney cell line

BVDV – bovine viral diarrhea virus

C – capsid or core protein

***$C_{1/2}$* –** protein concentration at $\Delta\zeta_{max}/2$ (half of the protein concentration needed for saturation)

***CC* (*t*) –** correlation coefficient of the *I*(*t*) function.

CD – circular dichroism spectroscopy

CNS – central nervous system

cryo-EM – cryo-electron microscopy

CSF – cerebral spinal fluid

***Cx* –** *Culex*

***D* –** diffusion coefficient

DENV – dengue virus

***D_H* –** hydrodynamic diameter

DLS – dynamic light scattering

DMEM – Dulbecco's modified Eagle's medium

E – envelope protein

EDTA – ethylenediamine-*N,N,N',N'*-tetraacetic acid

EGTA – ethylene glycol-bis(2-aminoethylether)-*N,N,N',N'*-tetraacetic acid

ESI-MS – electrospray ionization mass spectrometry

ER – endoplasmic reticulum

***F* –** force

$\boldsymbol{f(ka)}$ **–** Henry's function

$\mathbf{g_1}(\boldsymbol{t})$ **–** first order autocorrelation function

$\mathbf{g_2}(\boldsymbol{t})$ **–** second order autocorrelation function

HCV – hepatitis C virus

HDL – high density lipoprotein

HepG2 – human hepatocellular liver carcinoma cell line

HGV – hepatitis G virus

HPLC – high-performance liquid chromatography

***I* –** light scattering intensity

***I*(D_H) –** light scattering intensity distribution function of D_H

Ig – immunoglobulin

***I*(t) –** light scattering intensity as a function of time

$\boldsymbol{I_t}$ **–** light scattering intensity at time *t*

$\boldsymbol{I_{t+\Delta t}}$ – light scattering intensity at time $t + \Delta t$

***k* –** spring constant

Kv2.1 – a human K^+-specific channel

LD – lipid droplet

LDH – lactate dehydrogenase

LDL – low density lipoprotein

LDLR – low-density lipoprotein receptor

LVP – lipoviroparticle

M – membrane protein, maturates from the prM through the activity of the host furin protease

$\boldsymbol{n_0}$ **–** refractive index of the scattering material

***n*(D_H) –** particle number distribution as a function of D_H

NS – nonstructural protein

p7 – an HCV viroporin

PAT family – LDs protein family composed of PLIN1, ADRP and TIP47

pep14-23 – a rationally designed peptide with sequence NMLKRARNRV, protected under a patent application (WO 2012159187)

PLIN3 – perilipin 3

PMSF – phenylmethylsulfonyl fluoride

pre-VLDL – premature VLDL

prM – premature M protein

***q* –** scattering vector

SE – standard error

spp. – species

ss(-)RNA – single-stranded negative-sense RNA

ss(+)RNA – single-stranded positive-sense RNA

***T* –** absolute temperature

***t* –** time

TEE – buffer with 20 mM Tris-HCl, 1 mM EDTA and 1 mM EGTA, pH 7.4

TIP47 – tail-interacting protein of 47 kDa or perilipin 3, an LDs protein

VLDL – very-low density lipoprotein

WNV – West-Nile virus

WNV-K – WNV serotype Kunjin

Γ – decay rate

Δx – the length of the deflection of the cantilever in AFM-based force microscopy

Δζ – ζ-potential variation

$\Delta\zeta_{max}$ – maximum ζ-potential variation

$\boldsymbol{\varepsilon}$ **–** dielectric constant

$\boldsymbol{\eta}$ **–** dispersant viscosity

$\boldsymbol{\theta}$ **–** scatter angle

$\boldsymbol{\kappa}$ **–** Boltzmann constant

$\boldsymbol{\lambda}$ **–** electromagnetic radiation wavelength

$\boldsymbol{u}$ **–** electrophoretic mobility

$\boldsymbol{\beta}$ **–** an instrumental constant of the deviations from ideal correlation (β = 1)

Amino acid residues and sequences are indicated using the one-letter code. Amino acid residues may also be denoted by using the following symbols: “+”, for the positively-charged residues; “-”, for the negatively-charged residues; and “h”, to represent the hydrophobic conserved residues.

I - Introduction

In this chapter it is first presented appropriate information regarding West-Nile virus spread, mode of transmission and the main clinical manifestations of the infection, to contextualize the reader regarding the epidemiological significance of studying this expanding virus threat. Following, the relevant information concerning flaviviruses in general, West-Nile virus is depicted in particular, with a special emphasis in the viral life cycle and virion structure, as well as its capsid protein, the subject of study of this thesis. This protein is then discussed in terms of its structure and ability to interact with host lipid systems such as lipid droplets and very-low density lipoproteins. Finally, the main aims of this work are presented.

West-Nile virus epidemics and global impact

Spread and mode of transmission

West-Nile Virus (WNV) is a single-strand positive RNA virus of the *Flaviviridae* family that was first isolated in Uganda in 1937 (Kilpatrick, 2011). Since then, it became endemic across Tropical Africa, southern Asia and Northern Australia, with episodic occurrences in Europe (Kilpatrick, 2011). Despite its severity, WNV infection raised little concern until when an extremely virulent strain appeared in North America, at the turn of the millennium (Kilpatrick, 2011; Reiter, 2010; Rossi *et al*., 2010). This strain, originally found in 1999 in Brooklyn, New York, has quickly spread, in only 4 years having managed to invade most of North America (Kilpatrick, 2011; Rossi *et al*., 2010). Between 1999 and 2010, only in the USA, this resulted in over 1.8 million infected people, 12852 severe encephalitis/meningitis cases and 1308 deaths (Reiter, 2010). Mirroring the quick spread in USA, this highly virulent WNV strain can easily establish itself in Europe. Similarly to other flaviviruses (such as dengue and yellow fever viruses), the globalization of trade and travel has facilitated the spread of the original virus (Kilpatrick, 2011; Reisen, 2010; Reiter, 2010; Rossi *et al*., 2010). Since the virus is easily transmitted to humans via the bite of *Culex* spp. mosquito vectors feeding on infected birds, migratory birds constitute another major vehicle of transmission (Kilpatrick, 2011; Reisen, 2010; Reiter, 2010). In spite of the genus *Culex* being the key vector, 60 species of mosquito have been implicated in the transmission of WNV. In particular, mosquitoes found in North America and Europe (Figure 1.1) belong to the *C. pipiens* group (such as *C. pipiens pipiens*, *C. pipiens molestus,* and *C. quinquefasciatus*) and can drive the transmission of WNV (Gray and Webb, 2014).

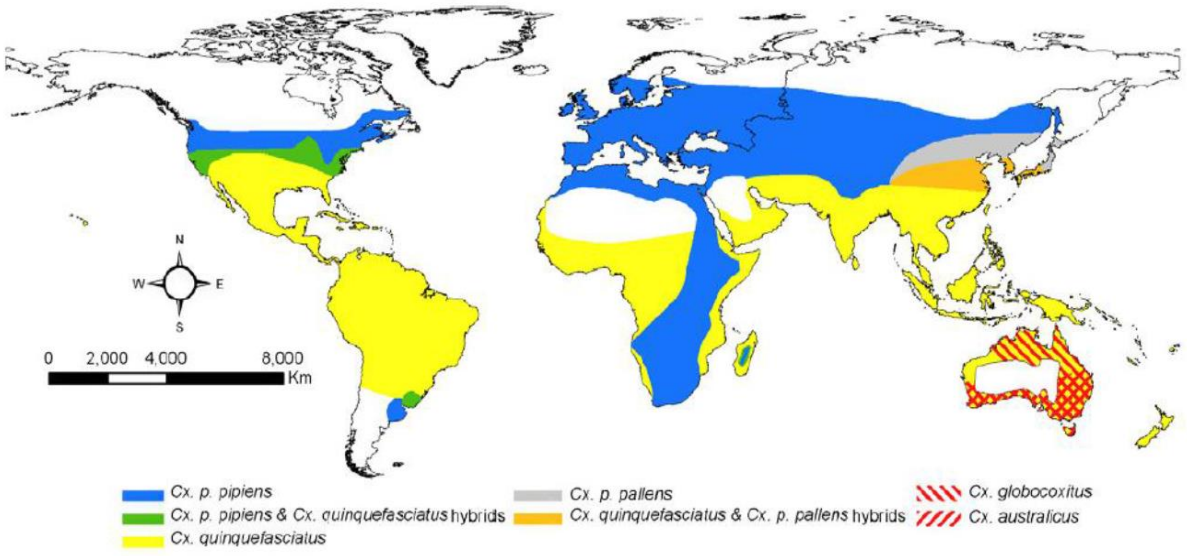

Figure 1.1 - Global distribution of *Cx. pipiens* complex mosquitoes. Geographic range for *Cx. p. pipiens* includes both forms (*pipiens* and *molestus*). *Cx. australicus* and *Cx. globocoxitus* are restricted to Australia (Ciota and Kramer, 2013).

As reviewed elsewhere (Kilpatrick, 2011; Gray and Webb, 2014), *Culex* spp. mosquitoes are predominantly ornithophilic species and are considered efficient enzootic vectors, bird-to-mosquito-to-bird transmission. However, as the mosquitoes are closely associated with urban environments there is an increased risk to act as epizootic vectors (bird-to-mosquito-to-human transmission). Members of the *C. pipiens* complex occur in both North American and Europe, although in North America, *C. tarsalis* is considered one of the major vectors of WNV, while in some regions of Europe *C. modestus* has been implicated as a locally important vector. Endemic mosquitoes may play a locally significant role in enzootic and in epidemic transmission of WNV. The variations in risk may be driven by differences in the availability of suitable mosquito habitats, relative abundance of *Culex* spp. mosquitoes and their host feeding preferences (Gray and Webb, 2014). The mosquito vectors are abundantly found in Europe and the number of bird species that can host the virus is considerable, given the surprisingly large range of taxa that WNV infects, including common European birds such as corvids, robins, chickadees and thrushes, among others (Kilpatrick, 2011).

Accordingly, a virulent strain can easily spread across Europe (Reisen, 2010; Bagnarelli *et al*., 2011; Barros *et al*., 2011). In fact, in the summer of 2011, 89 laboratory-confirmed human cases of WNV infection have been reported in the European Union (EU) (although, fortunately, not the most virulent strain): 66 cases in Greece, 13 in Italy and 10 in Romania. Another 149 cases occurred in neighboring countries with intense commercial relations with the EU (Bagnarelli *et al*., 2011). In 2012, there was resurgence in human cases in North America, with 5,674 patients reported with clinical illness in the USA and 428 clinical cases notified in Canada. North American WNV activity levels remained higher than historical averages in 2013, with 2,318 human disease cases reported in the US and 108 cases in Canada at the end of the transmission season. In 2012, there was a peak of 937 WNV cases in Europe and neighbor countries and in 2013, 783 WNV human cases, including 86 in Greece and 302 in Serbia, were reported (Gray and Webb, 2014). Figure 1.2 shows the distribution of WNV in Europe.

Typically, following a bite of a WNV infected mosquito, the virus first infects keratinocytes and Langerhans cells, which end up in regional lymph nodes, where the first round of the initial replication occurs (Johnston *et al*., 2000; Lim *et al*., 2011a). On a second stage, WNV titer becomes high enough for it to spread systemically to visceral organs, primarily infecting the kidney and the spleen (Johnston *et al*., 2000; Lim *et al*., 2011a; Tesh *et al*., 2005). Here, a second round of replication occurs, presumably in kidney epithelium cells and spleen macrophages (Samuel and Diamond, 2005; Johnston *et al*., 2000; Tesh *et al*., 2005). The disease progresses to the neuro-invasive stage only if high enough levels of viremia are achieved at this crucial stage (Samuel and Diamond, 2005; Tesh *et al*., 2005). In that situation of high WNV concentrations in the blood, the virus crosses the blood-brain barrier (BBB) causing meningo-encephalitis. This is similar to what has been observed for other neurotropic viruses, such as Saint-Louis encephalitis virus, where the probability of neuro-invasion appeared to correlate with the level and duration of viremia (Bowen *et al*., 1980). The interaction between WNV and components of the BBB have a significantly impact in the neuropathogenesis. When the BBB is compromised WNV can replicate in astrocytes, cells that have an important role in the homeostasis of the central nervous system (CNS) through the uptake of neurotransmitters and

other extracellular factors, as well in the integrity of the BBB. In fact, evidences show that WNV replication in astrocytes influences the results of viral infections of the CNS (Hussmann *et al*., 2014). Therefore, blocking the infection at visceral stage is critical for preventing its evolution to the life-threatening neurological stage (Diamond, 2009; Kimura *et al*., 2010; Lim *et al.*, 2011b; Rossi *et al*., 2010).

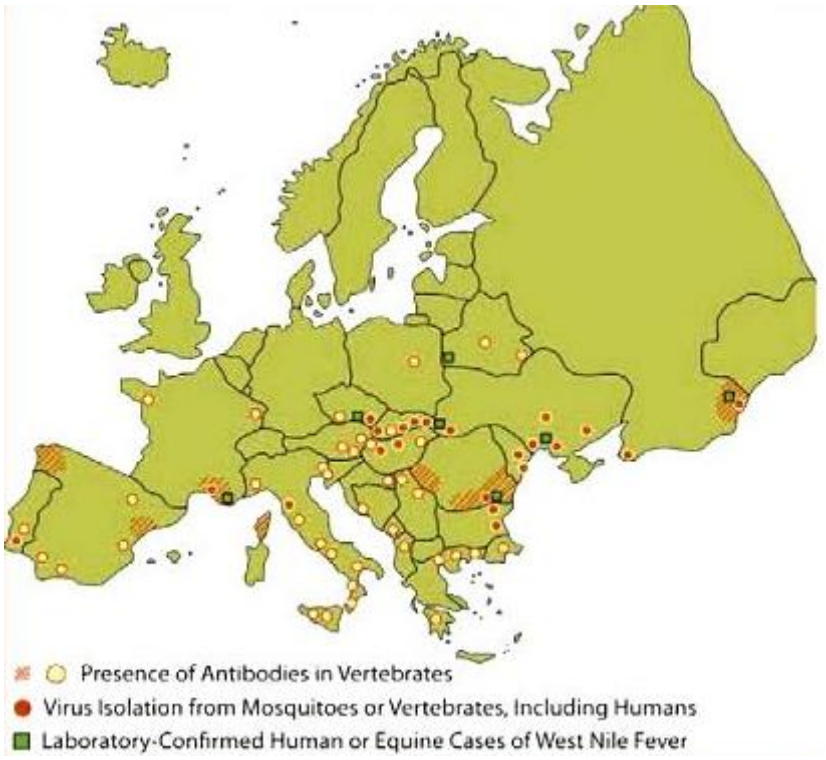

Figure 1.2 - **European distribution of West Nile Virus.** Sporadic cases of disease in horses and humans were observed occasionally in France, Portugal, Spain, Italy, Czech Republic, Romania, and Hungary (Pauli *et al*., 2013).

Symptoms and diagnosis

As recently reviewed elsewhere, (Sejvar, 2014) WNV infection can lead to a vast number of symptoms that in some cases can be confounded with a common febrile disease. In fact, in the first well-documented reported outbreaks of WNV in sub-Saharan Africa and the Middle East, the disease was characterized as a mild, self-limited illness that rarely progressed to a severe disease and almost never left any sequels (Campbell *et al*., 2002). Upon the emergence of WNV in North America and a more accurate detailed understanding of the disease course, it became clear that WNV infections can lead to a wide array of symptoms, including very severe clinical manifestations. Cases of neurologic illness were reported, in some cases with development of neuro-invasive disease (Sejvar, 2014). WNV infection can lead to mild symptoms common to other febrile diseases, such as fever and abdominal rash, or to a more severe clinical form of neuro-invasive disease that includes neck stiffness, stupor, disorientation, meningitis, paralysis, coma and death (Rossi *et al*., 2010). It is important to bear in mind that although WNV is now commonly known for the neurologic symptoms, the infection does not

always follows through to the final neuro-invasive stage (Diamond, 2009; Kimura *et al*., 2010; Lim *et al.*, 2011b; Rossi *et al*., 2010). It is estimated that 80% of WNV infections are mostly asymptomatic. Thus, only a small portion develops the symptoms of the systemic febrile illness known as West-Nile fever that gave the name to the virus. Regarding the neurological manifestations, only 1 % of the cases of WNV infection evolve to a neurologic illness, in which the virus infects the nervous system (Sejvar, 2014). There are three recognized types of neuro-invasive disease: aseptic or West-Nile meningitis, which involves infection of the meninges; West-Nile encephalitis, in which infection of the brain parenchyma occurs; and, finally, the acute poliomyelitis-like syndrome known as West-Nile poliomyelitis, that results in an acute flaccid limb weakness as the result of a viral infection of the anterior horn cells of the spinal cord (Campbell *et al*., 2002; Granwehr *et al*., 2004). The severity of WNV infection is highly dependent on the age of the infected person. Roughly, as a rule of thumb, for each decade of life it becomes 1.5 times more likely that the disease develops into the neuro-invasive stage (O'Leary *et al.,* 2004). However, children also can develop the neuro-invasive version of the disease, in most cases due to an infection of the meninges (Civen *et al.*, 2006; Lindsey *et al*., 2009). However, it is important to understand that sometimes the clinical manifestations can overlap and there is not a well-differentiated clinical picture. As such, the diagnosis of the clinical syndrome in persons with an overlap of manifestations of WNV is sometimes difficult. The diagnosis is even more complicated when other manifestations associated with WNV infection occur (Sejvar, 2014). It is possible that a large number of WNV infections go unreported, since diagnosis based on the clinical manifestations can therefore be somewhat difficult.

One of the most appropriate WNV diagnosis approach is based on the detection of immunoglobulin (Ig)M in serum or cerebral spinal fluid (CSF) (Gray and Webb, 2014). Although, IgM may be negative at the time of presentation, more than 98% of symptomatic patients only have a positive serum IgM about 3 to 8 days after the onset of symptoms (Gray and Webb, 2014; Wilson and Bale, 2014). Furthermore, WNV IgM may persist in the serum for years in some patients. Thus, the diagnosis and surveillance of acute infections can be difficult in these cases, particularly in the context of annual seasonal outbreaks (Murray *et al*., 2013; Papa *et al*., 2011). Generally, IgM antibody capture enzyme-linked immunosorbent assay is used. It can be applied to serum and CSF. In patients with previous *Flavivirus* infection or immunization the test result may not be correct (false positives may be seen). In these situations, it is better to employ the highly specific plaque-reduction neutralizing antibody assay (Gray and Webb, 2014). As specific IgM antibody generally only can be detected after the first week, the use of nucleic acid detection techniques provided an opportunity to diagnose WNV in patients prior to their clinical manifestation. This approach enables the detection of WNV RNA in the bloodstream (in average, 4 days prior to the first detection of IgM antibodies) and has become a routine test for screening blood products in endemic areas (Busch *et al*., 2008). It is important to understand that to reduce the risks of WNV a great mosquito control will be required, as well as sophisticate surveillance programs, and modification of human and environmental factors. Vaccination of horses has been implemented in some endemic regions but, however, no vaccine for humans has been registered so far (Gray and Webb, 2014).

West-Nile virus life cycle and structure

Viral life cycle

The life cycle of WNV is constituted by several steps that are similar for all viruses of *Flaviviridae* family (Figure 1.3), as thoroughly described elsewhere (Mukhopadhyay *et al.*, 2005). The WNV life cycle begins with attachment of the virus to the cell surface. In this step the viral envelope (E) interacts with cellular receptors. Subsequently, viruses are internalized by receptor-mediated endocytosis and transported to endosomes. Inside the cell, acidification of the endocytic vesicles with viral particles trigger conformational rearrangements in the virion that allows the fusion of the viral envelope (E) with the vesicle membrane. The viral genome ss(+)RNA is released in the cytoplasm and translated as a single polyprotein that it is cleaved by several viral and host proteases, originating ten viral proteins (seven non-structural proteins and three structural proteins) (Hussmann *et al*., 2014; Mukhopadhyay *et al.*, 2005). The three viral structural proteins, capsid (C), membrane (prM/M) and envelope (E), are encoded by that order at the beginning of the single open reading frame after which come the seven nonstructural proteins (NS1, NS2A, NS2B, NS3, NS4A, NS4B, and NS5) (Brinton, 2013). The viral genome serves as a template for replication. Non-structural proteins transcribe molecules of ss(-)RNA as a template for the synthesis of new ss(+)RNA (Urcuqui-Inchima *et al.*, 2010). Genome replication occurs on intracellular membranes. After the synthesis of the viral proteins and of viral RNA to a high level, the immature viral particles are formed: the viral genome is surrounded by the capsid (C) protein, precursor membrane (prM), and E proteins on the surface of the endoplasmic reticulum (ER) (Mukhopadhyay *et al.*, 2005). The prM protein protects the E protein (protein required for receptor binding, host membrane fusion and viral assembly) from the occurrence of an irreversible conformation change as the virion is secreted through acidified sorting compartments (Saiyasombat *et al*., 2014). The process of encapsulation and virus assembly is not well understood. The immature viral particles follow the cellular secretory pathway (Yu *et al*., 2008), within which prM is cleaved by furin-line proteases, promoting conformational changes that lead to the formation of mature virus particles. The maturation step may be determinant to WNV replication in some circumstances. Furthermore, the glycosylation of the viral particles may be determinant for the pathogenesis of WNV (Hussmann *et al*., 2014). Finally, the new virions can be released into the extracellular medium and are able to infect other host cells (Mukhopadhyay *et al.*, 2005).

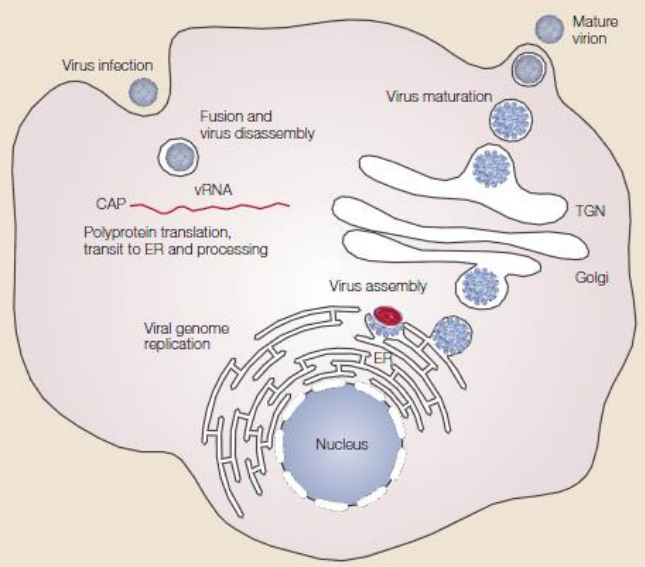

Figure 1.3 - *Flavivirus* life cycle. *Flavivirus* enter in the host cell by receptor-mediated endocytosis. Acidification of the endosomal vesicle conduct to the fusion of the viral and cell membranes and the genome ss(+)RNA is released into the cytoplasm. The ss(+)RNA is translated in a polyprotein that is processed by viral and host proteases, originating seven non-structural proteins and three structural proteins. Non-structural proteins promote the viral genome replication near the ER and structural proteins are involved in the viral assembly in the surface of the ER. After the virion maturation by the host protease furin, the mature virion follows the secretion pathway and subsequently is released by exocytosis (Mukhopadhyay *et al.*, 2005).

The virus structure

Members of Flavivirus genus, *Flaviviridae* family, to which WNV belongs, are structurally similar, with homologous proteins sharing highly conserved regions. In Figure 1.4, dengue virus (DENV) and WNV structures are shown, which are very similar. Flaviviruses such as WNV are icosahedral enveloped viruses composed of a lipid bilayer surrounding a nucleocapsid (Mukhopadhyay *et al.*, 2005). It should be noted that this structure is symmetrical, with no surfaces extensions. The nucleocapsid contains a positive sense single-stranded genomic RNA, forming complexes with multiple copies of the capsid (C) protein (Mukhopadhyay *et al.*, 2005), which are enveloped by a lipid bilayer. There are two other structural proteins associated to this lipid bilayer: the E and M proteins. Thus, the three structural proteins constitute the virus particle while the seven NS are involved in the viral replication, viral assembly and in the modulation of the host cells responses (Bhuvanakantham and Ng, 2013). It is important to note that WNV (Doklnad *et al*., 2004) and DENV (Ma *et al*., 2004) are particularly similar, especially in what respects their capsid proteins (Martins *et al*., 2012). From the three structural proteins, the C protein, essential for assembly and maturation of viral particles, is currently the most promising drug target candidate, given that previous approaches focused on the other two structural proteins have failed (Diamond, 2009; Kimura *et a*l., 2010; Rossi *et al*., 2010).

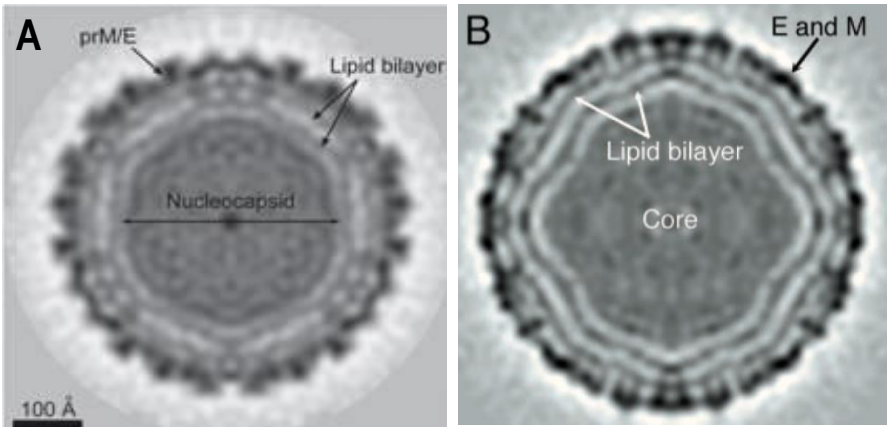

Figure 1.4 - Structures of dengue and West-Nile viruses determined by cryo-electron microscopy. (A) Cryo-EM image of a DENV particle. (B) Cryo-EM image of a WNV particle. Virion cores contain the nucleocapsid, where the viral genomic RNA is conjugated with multiple C protein copies; surrounded the nucleocapsid is a lipid bilayer derived from the host cell ER; the outer layer envelope is constituted by the E protein that is capped by the prM protein before maturation (Mukopadhyay *et al*., 2003; Yu *et al*., 2008).

The capsid protein

The *Flavivirus* capsid proteins are also highly multifunctional with other physiological roles besides being part of the core mature virion structure. WNV C can be localized in the cytoplasm and nuclei. The localization in the nuclei is dependent on the interaction with importins and a protein kinase C-mediated phosphorylation of arthropod-borne flaviviruses C proteins (Bhuvanakantham *et al*., 2010). The function of the C protein in the nucleus is not well understood, since it has been shown that nuclear phase is important for efficient virus replication (Bhuvanakantham *et al*., 2009), but it is known that ss(+)RNA replication occurs via cellular components in the cytoplasm (Bhuvanakantham and Ng, 2013). One of the most important processes of the virus life cycle, the virus assembly, is mediated by the C protein, ensuring the specific encapsidation of the WNV viral genome. In fact, this protein is involved in many other processes, as it acts as nucleic acid chaperone (Ivanyi-Nagy *et al*., 2008) and interacts with a variety of cellular proteins, modulating transcription, cellular metabolism, apoptosis and immune response (McLauchlan, 2000; Heaton *et al*., 2010; Ivanyi-Nagy *et al*., 2008; Netsawang *et al*., 2010).

The C proteins have roughly 100 amino acid residues (DENV C, for example, has 100 a.a., while WNV C has 105 residues). The C protein in solution forms a homodimer rich in α-helices, with each monomer composed by four α-helices (α1 – α4) connected by short loops (Dokland *et al.*, 2004; Jones *et al.*, 2003; Ma *et al.*, 2004). The WNV C protein has an asymmetric charge distribution, being a very positively charged protein due to the presence of only 3 negatively-charged residues and 26 arginine and lysine residues. One of the faces of the dimer is constituted essentially by positively-charged residues (α4 helices of each monomer), while the other face of the dimer is formed by non-charged and by non-polar residues (α1 and α2 helices of each monomer). It was proposed that the α4-α4' region is involved in the interaction with RNA and the α2-α2' region binds to molecular components of the viral membrane (Figure 1.5) (Ma *et al*., 2004). The first twenty residues of WNV C, as well the first twenty residues C protein of other *Flavivirus*, such as DENV C, are intrinsically disordered. The

flexibility conferred by their intrinsically disordered regions is expected to facilitate the functions in which flaviviruses C proteins are involved (Ivanyi-Nagy and Darlix, 2010). Importantly, as discusses in the next section, in several closely related members of the *Flaviviridae* family, such as DENV and hepatitis C viruses (HCV), the interaction of the homologous C proteins with intracellular lipid droplets (LDs) and with blood plasma very-low density lipoproteins (VLDL) is crucial for successful viral replication (Carvalho *et al*., 2012; Faustino *et al*., 2014; Martins *et al*., 2012; Mukhopadhyay *et al.,* 2005; Samsa *et al*., 2009).

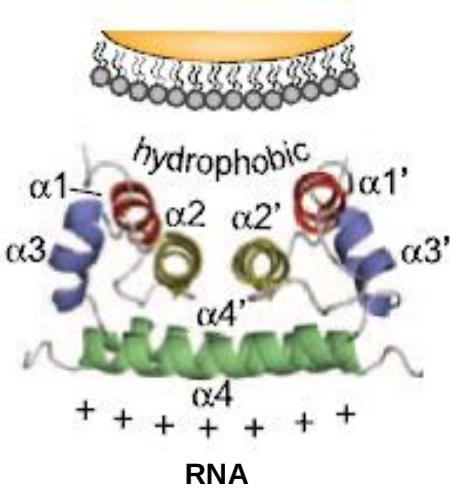

Figure 1.5 - Dimer structure of *Flavivirus* C proteins. The four α helices (α1 to α4) are indicated in each monomer. C proteins form an α-helical homodimer with an asymmetric charge distribution. The α2-α2' interface, highly hydrophobic, interacts with membranes and the α4-α4' region, mainly positively-charged, interacts with RNA. Adapted from Samsa *et al.*, 2009.

Lipid droplets and lipoproteins in *Flaviviridae* infections

Lipid droplets

Lipid droplets (LDs) are intracellular organelles that have also been referred as lipid bodies, oil bodies, adiposomes, oil droplets and fact bodies, specialize in the storage of neutral lipids (Ding *et al*., 2013). LDs are originated from the ER and are composed by a hydrophobic core of neutral lipid, mainly triacylglycerols and cholesteryl esters, surrounded by a monolayer of phospholipids and cholesterol, with a variety of proteins in the surface (Figure 1.6) (Lin *et al*., 2014). The diameter of LDs varies from 50 nm to 200 μm depending on cell type, but they always tend to have a globular shape. LDs provide the main cellular reservoir of lipids for energy storage (Krahmer *et al.,* 2009). In addition to storing energy, lipid droplets provide reservoirs of lipids (such as sterols, fatty acids and phospholipids) for hormone synthesis and membrane formation (Thiam *et al*., 2013), and protect cells from the lipotoxic effects of unesterified lipids (Krahmer *et al.,* 2009). The surface of LDs controls the accessibility of lipases to the stored triacylglycerols, since their utilization requires enzymatic breakdown by lipases (Lin *et al*., 2014). In the past decade, several studies have been developed to understand LDs biogenesis and functions. For that, several models systems, including bacteria, yeast,

green algae, *Caenorhabditis elegans*, *Drosophila*, plants and several types of mammalian cells and tissues have been used. The data collected show that LDs are very complex organelles and may be involved in lipid metabolism, membrane biosynthesis, membrane trafficking and signal transduction (Ding *et al*., 2013). Given their diverse functions, LDs are important organelles for cell homeostasis. With an important role in lipid storage, LDs also figure prominently in several pathologies due to lipid accumulation, such as obesity, fatty liver, type 2 diabetes and atherosclerosis (Krahmer *et al.,* 2013). In addition to phospholipids, the surface of LDs is decorated with several proteins (Krahmer *et al*., 2009; Thiam *et al*., 2013). Since the identification of perilipins as the major group of LDs surface proteins (with key roles in the regulation of lipid metabolism), proteomic and cell biology has revealed hundreds of LDs proteins in different cell types (Thiam *et al*., 2013). The main LDs proteins are from the PAT family: perilipin, adipose differentiation-related protein (ADRP) and tail-interacting protein of 47 kDa (TIP47), recently collectively renamed as perilipin 1, perilipin 2 and perilipin 3, respectively (Krahmer *et al*., 2009).

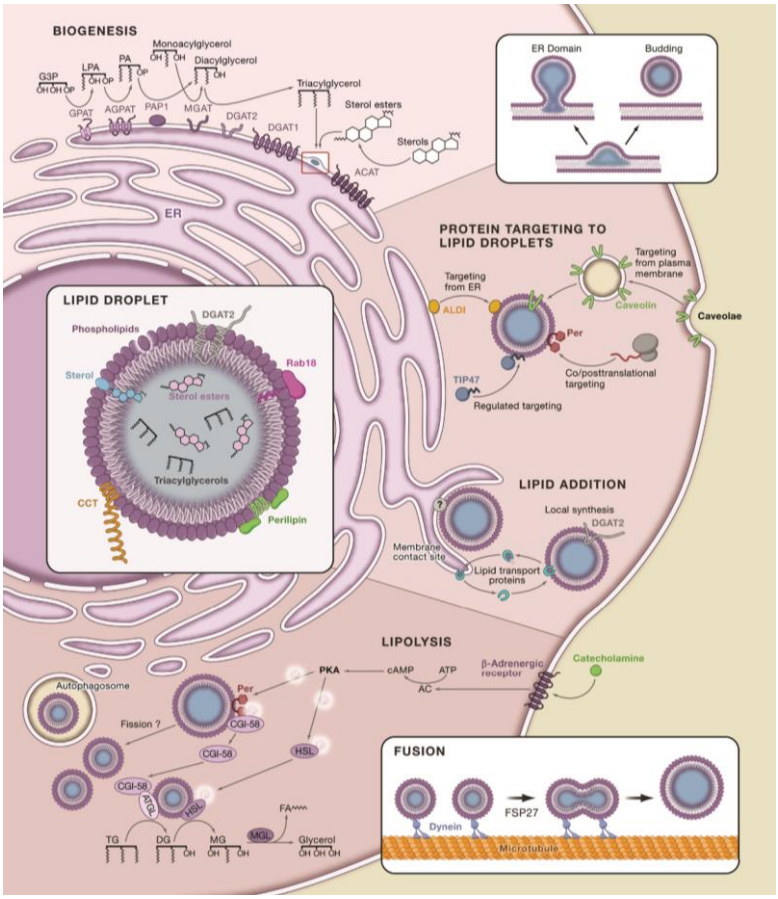

Figure 1.6 - LDs structure. LDs form at the ER, where the enzymes that catalyze neutral lipid synthesis are located. LDs structure comprises a neutral lipid core surrounded by a phospholipid monolayer that harbors small amounts of free cholesterol. Multiple proteins interact with the LDs surface through different structural features. The main LDs proteins are perilipin, ADRP and TIP47 (from the PAT family) (Krahmer *et al*., 2009).

Factors such as intracellular and extracellular stresses trigger LDs formation. In fact, accumulation of LDs occurs during progression of different pathologies (Pol *et al*., 2014). Several

important intracellular pathogens, such as DENV (Samsa *et al.*, 2009) and HCV (Barba *et al.*, 1997) also increase the formation of LDs in the host cells. It has been shown that TIP47 regulates HCV RNA replication through the interaction with a viral protein (Vogt *et al*., 2013). Viruses of the *Flaviviridae* family cause infections with liver steatosis, where it is notorious an increase in size and number of LDs in hepatocytes (Miller and Krijnse-Locker, 2008). Moreover, the C proteins of DENV and HCV, involved in viral assembly, associate with LDs during infection, a process essential for viral replication (Figure 1.7) (Assunção-Miranda *et al.*, 2010; Samsa *et al.*, 2009).

Several methods for isolating LDs have been established. These methods have been developed for proteomic and functional studies with LDs isolated from different species. The increase on the purity of LDs sample is one of the goals of the improving of these techniques, allowing the isolation of a reproducible amount of high-quality LDs (Ding *et al*., 2013).

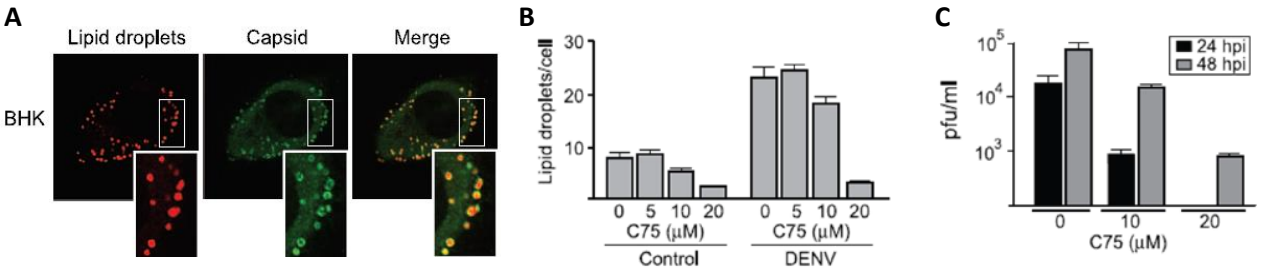

Figure 1.7 - Interaction of DENV C protein with LDs is required for DENV C replication. (A) Image of confocal microscopy: the C protein is targeted to LDs. DENV infected cells accumulate the C protein around LDs. (B) Effect of C75, an inhibitor of LDs formation, on the amount of LDs in BHK cells. The number of LDs decrease in cells infected and non-infected with DENV. (C) Viral replication was also inhibited. Adapted from Samsa *et al*., 2009.

Plasma lipoproteins

Blood plasma lipoproteins have also an important role in the life cycle of some *Flaviviridae* (Bartenschlager *et al.*, 2011; Survana and Rane, 2009). During *Flavivirus* infection, the composition and concentration of plasma lipoproteins are affected (Survana and Rane, 2009; van Grop *et al.*, 2002). Lipoproteins circulate in the bloodstream in suspension in the blood plasma, and are essentially classified in four major types, according to their density and function (ordered by decreasing average size and increasing density): chylomicra, very low density lipoproteins (VLDL), low density lipoproteins (LDL) and high density lipoproteins (HDL) (Cushley and Okon, 2002; Nelson and Cox, 2005).

Lipoproteins have key physiological functions, mainly on lipid homeostasis (Nelson and Cox, 2005). VLDL are mainly formed in the liver and distribute the lipids from there to all over the body, whereas LDs are responsible for the lipid homeostasis inside the cell. VLDL are quite similar to LDs in terms of structure and lipid composition, and both are derived from ER membrane. VLDL formation occurs on the luminal side whereas LDs are formed on the cytosolic side of the ER membrane. The main differences between these structures can be explained by the different formation pathways (Cushley and Okon, 2002; Nelson and Cox, 2005; Walther and Farese, 2009). LDL are generated from VLDL through delipidation, deproteinization and enzymatic metabolization in the bloodstream,

being therefore increasingly different from LDs (Cushley and Okon, 2002; Nelson and Cox, 2005). One of the major differences between LDL and VLDL is their protein composition (Table 1.1).

Table 1.1 - LDL, VLDL, LDs and LVP structure composition. The structure of all these systems is similar: a core of neutral lipids is surrounded by a monolayer of polar lipids where specific proteins are embedded. Their different lipid composition give them a different density. VLDL are very similar to LDs and lipoviroparticles (LVPs) in terms of lipid composition (Faustino *et al*., 2014).

Lipid system	LDL	VLDL	LDs	LVP[a]
Structure				
Density (g/mL)	1.019 – 1.063	0.930 – 1.006	–	~1.0
Diameter (nm)	18 – 25	30 – 80[b]	100 – 1000[c]	20 – 80
Cholesterol (%)	50	20	20	15
Triglycerides (%)	10	50	50	45
Phospholipids (%)	20	20	20	15
Proteins (%)	20	10	10	25
Proteins	ApoB100	ApoB100, ApoE, ApoC-I, ApoC-II, ApoC-III	Perilipin 1, Perilipin 2, Perilipin 3	ApoB100, ApoE, ApoC-I, C-II, C-III, Envelope, Capsid

a LVP are formed during HCV infection and they may be a common feature among flaviviruses.
b Premature VLDL (pre-VLDL) and VLDL in pathological conditions can exceed 200 nm in diameter.
c LDs larger than 1 µm usually occur in adipocytes, in fatty acid induced cells or pathogen-infected cells.

The main protein found in LDL is apolipoprotein (apo) B100. apoE is not found in significant quantity on the surface of LDL. VLDL have significant amounts of apo E, C-I, C-II and C-III, being enriched in different proteins on their surface. In fact, there are specific similarities between VLDL apoE and LDs protein perilipin 3 (PLIN3) (Hickenbottom *et al.*, 2004). Strikingly, despite their different physiological functions and locations, these proteins are structurally similar, having also sequence similarities. Through the comparison of the sequences and the structures of apoE and PLIN3, it is clear that apoE N-terminal and PLIN3 C-terminal regions are particularly similar (Figure 1.8). These features of lipoproteins might explain their role in the life cycle of different flaviviruses. HCV is able to fuse with premature very low-density lipoproteins (pre-VLDL) in the ER, during viral assembly and maturation forming lipoviroparticles (LVPs) (André *et al.*, 2002; Bartenschlager *et al.*, 2011). LVPs are released in the bloodstream as the normal lipoproteins (Bartenschlager *et al.*, 2011) and enter in the cells by the low-density lipoproteins receptor (LDLR) (Agnello *et al.*, 1999). LVPs are lipoprotein-like structures enriched in triacylglycerols that contain a viral nucleocapsid core and viral envelope proteins at the surface, as well as human apolipoproteins. LVPs have the particularity of being able to evade host defenses, being highly infectious (Bartenschlager *et al.*, 2011). Other *Flavivirus* can infect cells through the LDLR pathway, such as hepatitis G virus (HGV) and bovine viral diarrhea virus (BVDV). DENV infection can impair the host lipid metabolism, affecting the lipoproteins blood levels, especially in acute dengue hemorrhagic fever cases (Survana and Rane, 2009; van Grop *et al.*, 2002).

Recently, it was reported that DENV C can interact specifically with VLDL, eventually forming lipoviroparticles (Faustino *et al*., 2014).

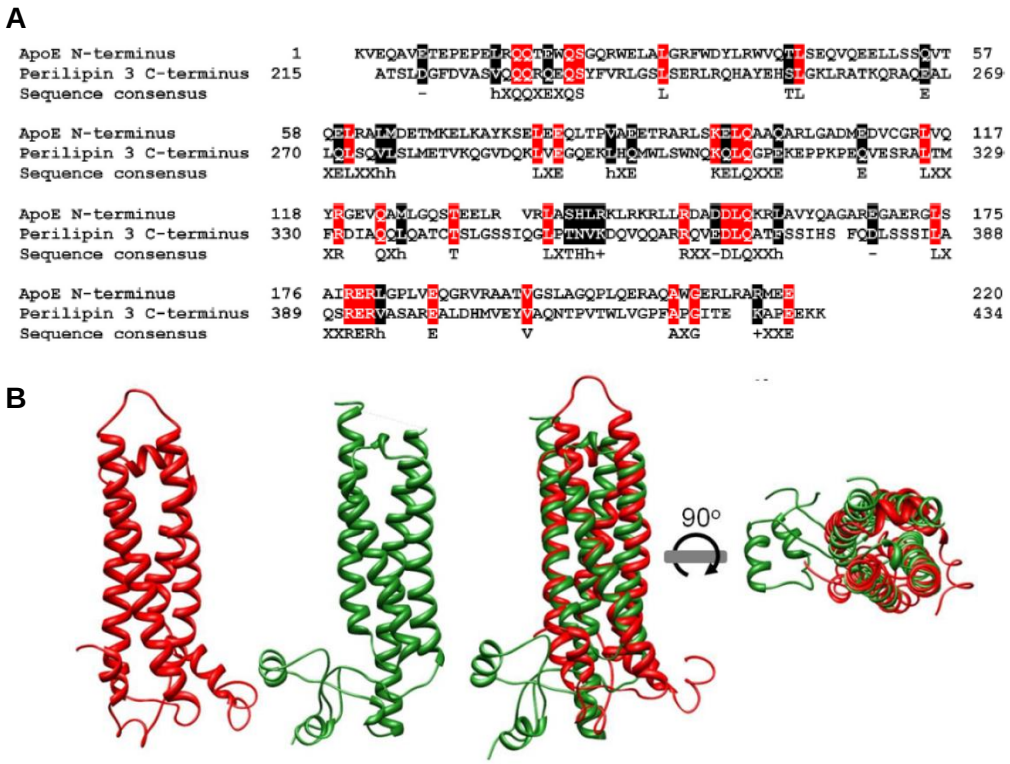

Figure 1.8 - Sequence and structural similarity between apoE N-terminus and perilipin 3 C-terminus. (A) Sequences of apoE N-terminus (first 220 residues) and perilipin 3 C-terminus (last 220 residues) show several similar regions, which could be involved in similar functions/interactions. Equal residues present in both of the aligned sequences (red); stereochemically and/or functionally identical residues (black). In the sequence consensus, "h", "+" and "–" stand respectively for hydrophobic, positively-charged and negatively-charged residues at the same aligned position. (B) The structures of apoE N-terminus (PDB ID: 2KC3 [red]) and perilipin 3 C-terminus (PDB ID: 1SZI [green]) superimpose in space through its common four-helix-bundle motif. Adapted from Faustino *et al.*, 2014.

Rationale for the study of WNV C protein interaction with lipid systems

Understanding the crucial steps of *Flavivirus* life cycle, such as the mode of interaction of the virus with the host cells components, in particular with lipid systems, can contribute to the development of effective drugs capable of inhibiting viral replication. It was already noted that in several RNA virus infections, such as those caused by DENV and HCV, the lipid metabolism is affected (Barba *et al.*, 1997). When *Flavivirus* infect a host cell their genome replicates in association with cellular membranes. In fact, it was shown that for the dengue and hepatitis C viruses, interaction of the capsid protein with host intracellular lipid droplets is crucial for viral replication (Counihan *et al*., 2011; Samsa *et al*., 2009). Recently, the host laboratory identified the DENV C amino acid residues responsible for its interaction with LDs (Martins *et al*., 2012) and showed also that specific protein components of LDs surface are involved in the interaction (Carvalho *et al*., 2012). In addition, it was

demonstrated that DENV C selectively interacts with VLDL, which may lead to the formation of LVPs (Faustino *et al.*, 2014). With this information the host laboratory successfully designed pep14-23 (Martins *et al*., 2012), a peptide inhibitor of dengue virus capsid protein interaction with LDs and VLDL (Faustino *et al.*, 2014; Martins *et al*., 2012). The inhibitor is based on a segment of DENV C that is highly conserved on WNV C (Martins *et al*., 2012). In fact, the sequence and the structure of C proteins seem to be conserved among *Flavivirus* (Figure 1.9) (Martins *et al*., 2012).

It is known that viruses have evolved several strategies to manipulate cellular functions during infection (Bartenschlager *et al.*, 2011; Samsa *et al*., 2009). Viral proteins have different activities and properties, associated to their high structural flexibility. This high structural flexibility is in part due to the presence of intrinsically disordered regions, which allow the interconverting of structures with a lack of a defined folding. Usually, disordered regions are involved in functions that need structural flexibility, such as recognition, regulation, signaling and interaction with nucleic acids and proteins. As mentioned before, the C proteins of *Flavivirus* form symmetric homodimers in solution and can interact with RNA and lipid systems. In fact, the segment containing the first 20 amino acid residues in C protein was found to be disordered in solution, in both WNV and DENV C proteins. C proteins structure and surface charge distribution enable capsid assembly through the interaction with lipid membranes by the central hydrophobic region in the α2-α2' interface and can interact with the viral RNA by the positively charged α4-α4'. In detailed studies, the region in the N-terminal of DENV C that allows the interaction with endoplasmic reticulum-derived organelles was identified, an important process crucial for virus replication and the formation of infectious particles. As discussed before, no specific treatment is available for WNV infection. Due to the clear similarity between WNV and DENV C proteins, the understanding of the WNV life cycle, especially of the WNV C biological activity by following similar approaches to those used by the host lab regarding DENV C function is highly promising. Clarifying the biological activity of the WNV capsid protein may pave the way for future treatments against this and other related viruses.

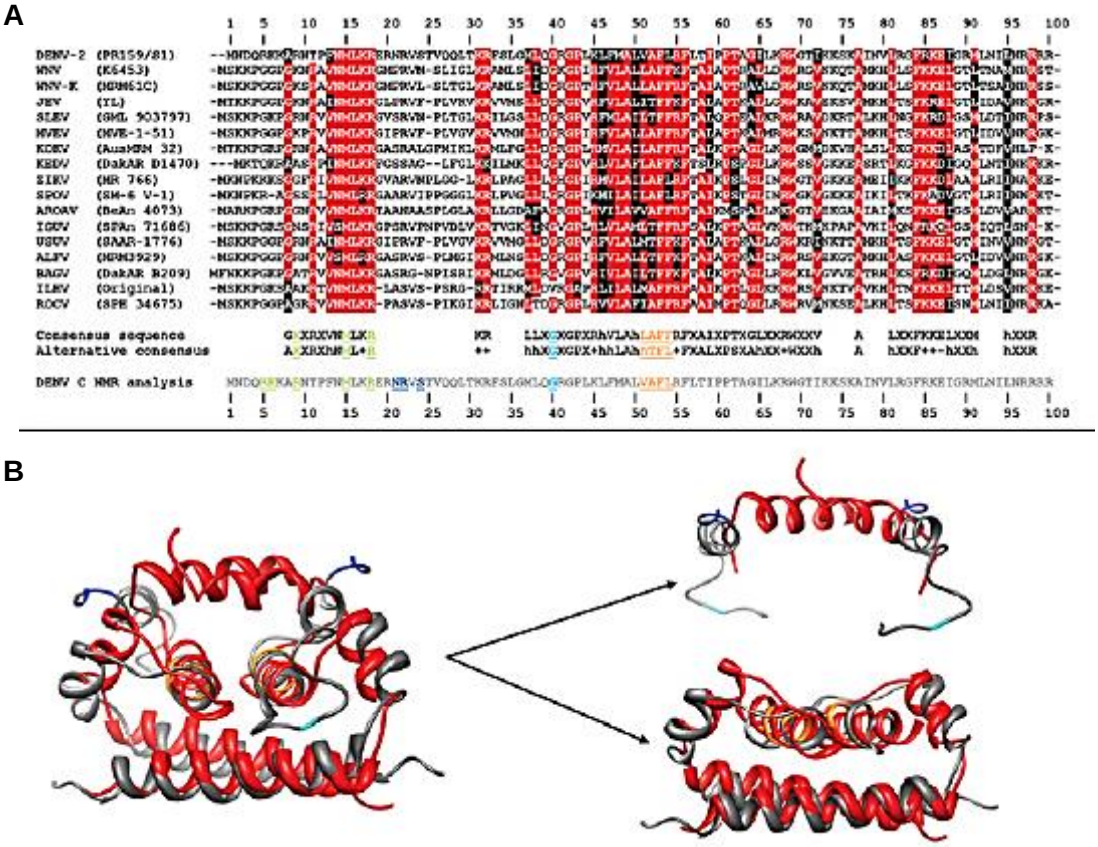

Figure 1.9 - C protein residues involved in the LD interaction are conserved among *Flavivirus* spp. (A) Alignment of the DENV C protein sequence with C protein sequences from other flaviviruses, highlighting fully conserved segments (red) and partially conserved residues (black). (B) Comparison of C protein structures of DENV (grey) and WNV-K (red). Two regions can be depicted: a conserved fold (from residues 44 to the C-terminus), and a particularly flexible region with alternative folds, containing α1 and the disordered section (residues 1–26). Adapted from Martins *et al*., 2012.

Aims and Goals

The studies developed in the last years in the field of *Flaviviridae* conducted to significant advances in the understanding of the life cycle of these viruses, in particular DENV. These findings resulted in the development of strategies to inhibit the crucial interaction of key viral proteins with the components of host cells, more specifically, in the potential use of pep14-23 or its derivatives to inhibit the interaction of DENV C with LDs and VLDL. However, this strategy may have wider applicability. The capsid proteins of other flaviviruses may interact with lipid systems in the same way that has been described for DENV C. Here the aim is to understand if the interaction of another *Flavivirus* C protein, WNV C, with host lipid systems also occurs. If so, pep14-23 may also function as an effective inhibitor of this key step of the flaviviruses life cycle.

In this study the aim is to unravel the mode of interaction of WNV C protein with relevant lipid systems, using a combination of biophysical techniques beneficial for the advance of the fundamental knowledge regarding the virus. To achieve the objective, first it was characterized the interaction of WNV C protein with lipid droplets (isolated from a kidney cell line), mimicking *in vivo* conditions as closely as possible. This characterization was performed via zeta-potential measurements, to quantify the role of charges in the interactions, as well as to quantify the binding affinity, and with atomic force microscopy (AFM)-based force spectroscopy, which allows the characterization of the interactions at the single-molecule level. Secondly, the interaction of WNV C with lipoproteins isolated from human blood plasma (VLDL and LDL) was also studied by AFM-based force spectroscopy, and by dynamic light scattering (DLS) to determine the size increment of the WNV C-VLDL complexes. Finally, DLS measurements were performed to test the possible ability of pep14-24 to inhibit the WNV C-VLDL interaction.

II - Methodology

This chapter contains a brief introduction to the basic aspects of the main biophysical techniques employed is this study: zeta potential, dynamic light scattering and AFM-based force microscopy. Following, the experimental procedures and the sources of the materials used are described, with particular detail for the LDs production, isolation and purification procedure.

Biophysical techniques

Dynamic light scattering

Dynamic light scattering (DLS) is the technique most commonly used to determine the size distribution profile of particles in suspension (Domingues *et al*., 2008). However, it is important to consider that different factors may affect the particle size distribution measured by DLS, such as the concentration of the suspension and composition of solvents (Yang *et al.*, 2014). Another important point is aggregation. It may occur in the sample solution or suspension during its preparation, or during measurements. In these cases, DLS may give inaccurate and unreliable results on the size of individual particles, as smaller particles can form agglomerates which can be identified or counted as one large particle. Aggregation usually occurs due to an imbalance of repulsive electrostatic forces and attractive van der Waals forces (Hinterwirth *et al*., 2013; Yang *et al.*, 2014). Other methods are used to size determination, such as microscope techniques, size-exclusion chromatography, differential mobility analysis and field-flow fractionation. All these methods have its specific shortcomings (Hinterwirth *et al*., 2013). DLS is able to give accurate values for particle size ranging from 1 nm to 1 µm, depending on sample, equipment and other experimental conditions (Domingues *et al*., 2008).

DLS is used to measure particle hydrodynamic diameter and size distribution of molecules or supra-molecular aggregates based on the light scattering intensity fluctuation on a small volume in a time-scale of microsecond, due to the Brownian motion of the particles (Figure 2.1) (Domingues *et al*., 2008). Brownian motion is the random zigzag motion caused by collisions with solvent molecules, which are themselve randomly moving owing to their thermal energy. Hence, the velocity of the particles in suspension is proportional to the particle mass (product of the size and density) (Uskoković, 2012). Size determinations can be performed through the measurement of the scattering light intensity fluctuations as a function of the time ($I(t)$). The diffusion coefficient is measure employing an autocorrelation function ($g_2(t)$) (Santos and Castanho, 1996):

$$g_2(t) = < I_t . I_{t+\Delta t} > \quad \textbf{(1)}$$

where I_t are a point of the $I(t)$ function at time t and $I_{t+\Delta t}$ another after a short time period Δt. This is the multiplication of the number of photons that arrives the detector at two successive time intervals and this calculation is repeated hundreds of thousands of times.

Considering the normalized scattered electric autocorrelation function ($g_1(t)$), it is possible determine the diffusion coefficient (D) of the particle from the decay rate (Γ) and the scattering vector (q) of the intensity function with the relation (Berne and Pecora, 1990):

$$g_1(t) = e^{-\Gamma t} \quad \textbf{(2)}$$

with:

$$\Gamma = Dq^2 \quad \textbf{(3)}$$

$$q = \frac{4\pi n_0}{\lambda} \sin\left(\frac{\theta}{2}\right) \quad \textbf{(4)}$$

where n_0 is the refractive index of the scattering material, λ the wavelength of the scattered light and θ its angle. It is important keep in mind that the diffusion coefficient (*D*) depends not only on the size of the particle, but also on other factors, such as the topology and chemical ordering of the particle surface, as well as the ionic strength and the ionic composition of the medium (Uskoković, 2012).
$g_2(t)$ is related with the first order autocorrelation function ($g_1(t)$) via the Siegert relation (Santos and Castanho, 1996):

$$g_2(t) = < {I_t}^2 > . \beta . g_1^2(t) + < I_t >^2 \quad \textbf{(5)}$$

where β is an instrumental constant of the deviations from ideal correlation (β = 1).

To calculate the correlation kinetics, which depends on the intensity-weighted diffusion coefficient (*D*), different methods can be employed, such as CONTIN or Cumulants. CONTIN is a numerical method which use a multiexponential correlogram fit to assess *D* distribution in solution. Cumulants uses a monoexponencial correlogram fit to obtain an average *D*. With the Stokes-Einstein equation, it is possible determine the hydrodynamic diameter (D_H) from *D* value (Berne and Pecora, 1990):

$$D_H = \frac{\kappa T}{3\pi\eta D} \quad \textbf{(6)}$$

where η is the dispersant viscosity, κ the Boltzmann constant and *T* the absolute temperature. It should be noted that the exponentially decaying curve goes to zero at time when the particle in movement exceeds the wavelength of the laser light (Uskoković, 2012).

The scattering intensity distribution function of D_H ($I(D_H)$) is obtained, and can be converted to $n(D_H)$, the particle number distribution function of D_H through the Mie theory. The scattering intensity of a particle is proportional to the sixth power of its D_H (Rayleigh's approximation); thus, the conversion can be done by the following transformation:

$$n(D_H) \approx \frac{I(D_H)}{{D_H}^6} \quad \textbf{(7)}$$

$n(D_H)$ expresses how much a particle of a certain diameter scatters light.

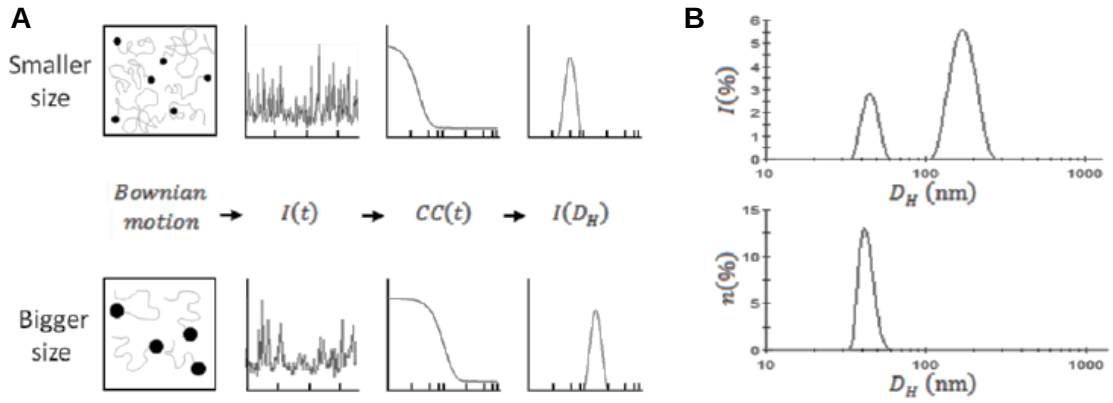

Figure 2.1 - Dynamic light scattering principle. (A) Particle size can be determined through the measurement of the scattering light intensity fluctuations as a function of the time *I* (t). Each intensity value is correlated with the others, through autocorrelation functions (*CC*(*t*) is the correlation coefficient of the *I*(*t*) function). Larger particles generate higher correlation than smaller ones, because their motion is slower. Through the autocorrelation function and the Stokes-Einstein equation, D_H can be determined. (B) The intensity function of D_H can be transformed in the particle number distribution of D_H.

Zeta Potential

Zeta potential (ζ-potential) measurements are based on the concept that charged particles suspended in a solution attract to their surface ions with opposite charge, to which they can be strongly bound. These surface-bound ions form a layer, the Stern layer (Uskoković, 2012). Beyond the Stern layer another layer is formed, where ions diffuse more freely. When the particle moves in the solution, the ions strongly attached to their surface move with it whereas the ions in the diffuse boundary do not move with the particle. The potential that exists at this boundary is defined as the ζ-potential (Figure 2.2) (Domingues *et al*., 2008). However, the exact location of the shear plane is an unknown feature of the electric double layer. ζ-potential is normally considered a bit lower than the potential at the boundary of the Stern layer. In fact, the two potentials can be considered identical without produce a significant error. Only at high surfaces potentials and high electrolyte concentrations the difference between the two potentials can be pronounced (Uskoković, 2012).

The ζ-potential is calculated through the electrophoretic mobility of the particles in solution, on an electric field, to the electrode of opposite charge (Kirby and Hasselbrink, 2004). The viscous forces oppose the movement of the particles in suspension until reaching the equilibrium, and therefore a constant velocity. The electrophoretic mobility can be calculated by laser Doppler velocimetry in Zeta-sizer devices. In this case, the particle velocity is related to the frequency measured by intensity fluctuation on the scattered light, or based on phase analysis light scattering. The first method has the disadvantage that the sensitivity of the Doppler Effect to the low mobility of large particles is very low, hindering the calculation of electrophoretic mobility. Other problem it is the measure of the mean square displacement of the particles instead of the mean displacement. Calculating the electrophoretic mobility basing on phase analysis light scattering is more accurate. With this technique it is possible measure differences in phase between the reference beam and the sample-scattered shifted beam

(phase shift is related to the position of the particle) (Domingues *et al*., 2008). The mean phase change with time yields the electrophoretic motion (Miller *et al*., 1991).

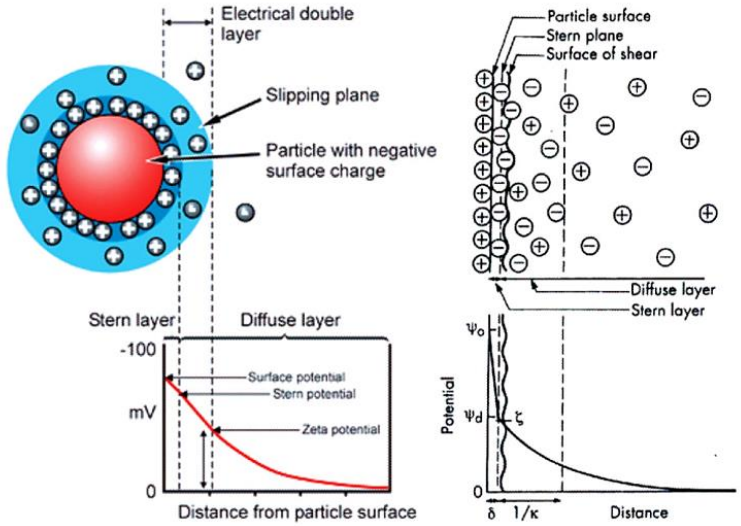

Figure 2.2 - ζ-potential of a particle: distribution of counterions in the double layer surrounding a negatively charged particle. The ζ-potential of a particle is proportional to its surface charge. The particle negatively charged in suspension attracts counterions of the solution to their surface, which forms the Stern layer. This layer of counterions is depicted as tightly bound to the charged particle surface. The electric potential between the second layer boundary of the shear plane and the solution is the ζ-potential. When an electric field, which changes the polarity with a given frequency, is applied to the solution, the particles move and the phase shift in the scattered beam is measured along time (Uskoković, 2012).

The ζ-potential of the particles can be calculated using the Henry's relation:

$$\zeta = \frac{3\eta u}{2\varepsilon f(ka)} \quad \textbf{(8)}$$

where ζ is the ζ-potential, u the electrophoretic mobility, η the viscosity of the solvent, ε its dielectric constant and $f(ka)$ is the Henry's function. When the particles are suspended in aqueous solutions with high ionic strength, the Henry's function is considered to be 1.5 (Smoluchowski's approximation); otherwise, if non-aqueous solutions are used, the value of this function is assumed to be 1 (Huckel approximation). The ζ-potential may be determined accurately for measurements with samples with particle sizes between 5 nm and 10 µm (Domingues *et al*., 2008).

.

Atomic force microscopy-based force spectroscopy

Atomic force microscopy (AFM) is one of the techniques from the group of scanning probe microscopies (Carvalho and Santos, 2012). This type of techniques consists in the scanning of a sample surface by a probe, measuring in this case the interaction force between the sharp tip and the surface (Santos and Castanho, 2004). This interaction force depends essentially on three parameters: the sample nature, the probe tip and the distance between them. To scan the surface the tip can do two different movements: drag across the surface or vibrate as it moves along it (Whited and Park,

2014). Typically, AFM is used for the construction of surface images. A tip attached to a flexible cantilever scans or taps the surface, while a laser beam reflected on the back of the cantilever is detected with a position-sensitive photodiode (Figure 2.3). Initially, the laser is pointed at the center of the photodiode, usually composed for four quadrants. When the sample is scanned, any small deflection on the cantilever will change the position of the reflected laser (lateral and vertical deflections of the tip are distinguishable). These deflections of the tip are processed by the electronic system and the sample surface topology is determined. AFM is a powerful tool, since it is able to measure a large range of orders of magnitude (Vahabi *et al.*, 2013). Furthermore, it has the capacity of imaging in air and in liquid, as well as in non-conductive and conductive surfaces. However, AFM can do more than only allowing the construction of images of surfaces. It can take advantage of its piconewton sensitivity, becoming a powerful tool for the study of molecular interactions, quantifying interaction between the tip and a specific spot in the sample. This approach is termed force spectroscopy (AFM-based force spectroscopy, to distinguish from other related approaches, using for instance optical or magnetic tweezers) (Carvalho and Santos, 2012; Vahabi *et al*, 2013; Whited and Park, 2014).

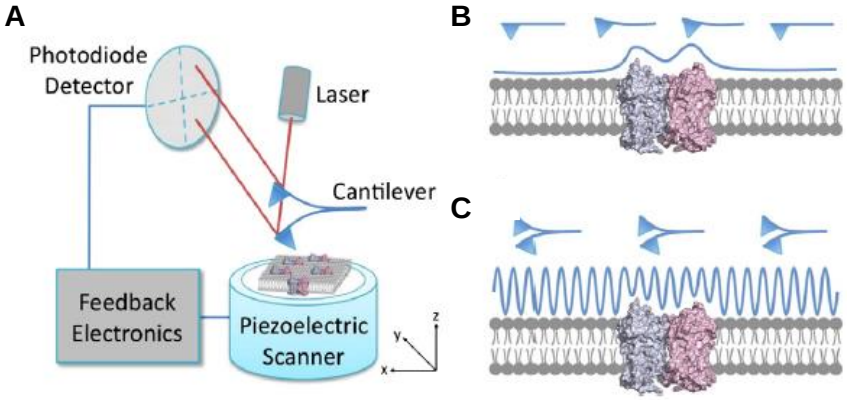

Figure 2.3 - Components of an atomic force microscope and different tip (or sample) movements. (A) AFM technique is based on the force applied by a nanometer-sharped tip, which can be functionalized, on the sample surface. A laser is reflected on the cantilever surface and its deflection can be measured with a photodiode detector. To scan the surface, the tip can do two different movements, (B) drag across the surface to a contact mode imaging or (C) vibrate as it moves along the surface to an intermittent contact mode imaging. In some equipments, to achieve these types of imaging, it is the sample holder that moves, while the tip remains on the same position (Whited and Park, 2014).

AFM-based force spectroscopy is a technique, that with their piconewton resolution, allows the measurement of inter- and intramolecular interaction forces required to separate the tip from the sample, enabling the detection of specific interaction forces at the single molecule level. For this type of studies the tips are functionalized with a probe molecule to recognize a specific target on the sample surface (Carvalho and Santos, 2012; Whited and Park, 2014). In AFM-based force spectroscopy measurements at the single-molecule level, normally the tip is brought into contact with the sample surface and retracted. For this, the cantilever moves first toward the surface and then in the opposite direction (in the z axis). The cantilever deflection of the vertical displacement of the piezoscanner can be recorded as a cantilever deflection versus scanner displacement curve. Briefly, the tip approaches the sample and a curve is generated with no variation in the force. When the tip

touches the sample, the force applied increases, leading to the deflection of the cantilever. Then, the tip retracts and a curve with the same appearance of the approach is generated. If a molecule attached to the tip, or simply the tip, adheres to the the sample, a binding event occurs and the retraction curve presents a different shape (Figure 2.4). This information can be converted into a force-distance curve using the Hookes's law of elasticity:

$$F = -k\,\Delta x \qquad \textbf{(9)}$$

where *F* is the force, *k* the spring constant of the cantilever and ∆x the length of the deflection of the cantilever. The tip, sample and medium composition influence the curve obtained. The covalent coupling of biomolecules to the AFM tip is other point to take into account for the force measurement. It is essential that the molecules can be removed from the surface during the retraction curve, but not from the tip (Carvalho and Santos, 2012).

In the present study, AFM-based force spectroscopy was performed to measure interactions of WNV C protein (covalently attached to the AFM tip) with LDs and lipoproteins (lightly adsorbed to a mica surface). The use of glutaraldehyde as a flexible cross-linker to couple the WNV C to the tip allows that the protein diffuses freely and its binding sites are available to form bonds with its ligands (Willemsen *et al.*, 2000). By tapping with this functionalized tip on the surface of the deposited sample, the detection of binding events and the probing of the force necessary to break the interaction can be determined at the single-molecule level. The number of proteins bound to the functionalized tip is unknown; however, it is not crucial for force measurements, since it is possible to identify single-molecules binding from the shape of the retraction curve. To have data statistically validated, it is necessary the acquisition of hundreds or thousands of curves, and the use of more than one AFM tip for each condition. With this information, histograms of distribution of rupture forces or distances can be generated and the frequency of (un)binding events calculated, from the number of curves with (un)binding events over the total number of curves obtained.

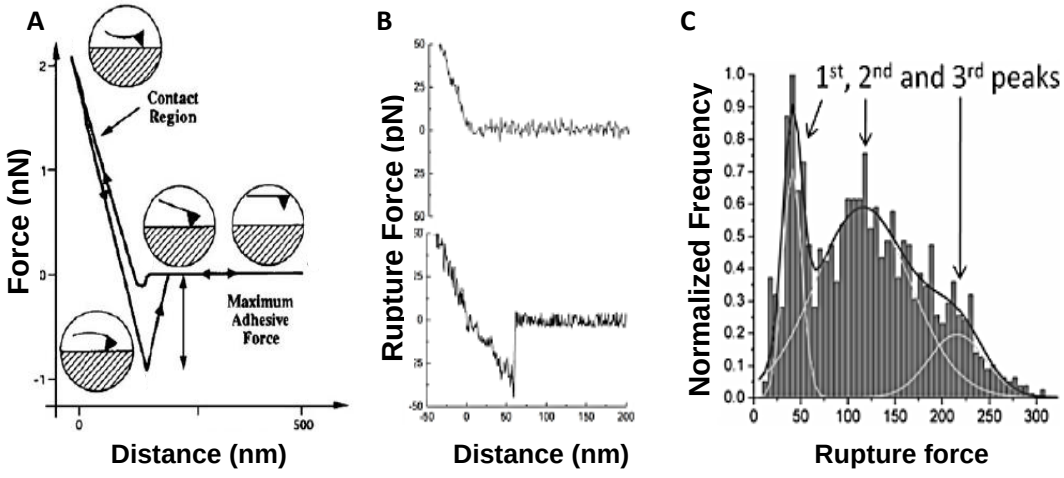

Figure 2.4 - AFM-based force microscopy. (A) Schematic diagram of a typical force-distance measurement cycle. With a protein functionalized tip (a tip functionalized with WNV C in this case), performing approach and retraction cycles on the sample (LDs and plasma lipoproteins in the present study), the force and distance necessary for the unbinding event are measured. When no interactions are observed, a curve as in the top of panel B is generated; if the protein binds to the sample surface, a curve as in the bottom of panel B is generated. With the information from hundreds or thousands of these curves, the histograms (C) are generated, in order to calculate the interaction parameters.

Material & Methods

Materials

Human plasma lipoproteins were obtained from Kalen Biomedical LLC (Montgomery Village, MD, USA). VLDL and LDL were isolated from human plasma by ultracentrifugation. The purified VLDL and LDL were ultrafiltered through a membrane and packaged aseptically under nitrogen (purity >97%). Both lipoproteins were provided in a solution with 154 mM NaCl, 5.6 mM Na2HPO4, 1.1 mM KH2PO4 and 0.34 mM EDTA at pH 7.4. VLDL ($d \leq 1.006$ g/mL) and LDL ($d = 1.019 – 1.063$ g/mL) where purchased at 1 mg/mL and 5 mg/mL concentration, respectively, and stored at 4 ºC. pep14-23 (H-NMLKRARNRV-NH2), a peptide rationally designed at the host lab and protected under an international patent application (WO 2012159187) was custom synthesized by JPT Technologies GmbH (Manheim, Germany) with > 95% purity, as confirmed by reverse-phase HPLC and ESI-MS analysis. WNV C protein (MSKKPGGPGKSRAVNMLKRGMPRVLSLTGLKRAMLSLIDGRGPTRFVLA LLAFFRFTAIAPTRAVLDRWRSVNKQTAMKHLLSFKKELGTLTSAINRRSSKQKK) was synthesized by VCPBIO (Shenzen, China) with 96.71% purity. Synthetic DENV C protein was also obtained through the same supplier. The secondary structure of synthetic DENV C was confirmed by circular dichroism spectroscopy (CD) to be identical to recombinant DENV C protein (obtained through a collaboration with the Federal University of Rio de Janeiro, Brazil). Full-length WNV C CD spectrum was also evaluated. Overall, the CD spectra observed for synthetic and recombinant DENV C are identical and rich in α-helical structure, while full-length WNV C also presents random coil content as well as α-helix (supplementary figure 1 of annexes), in line with previous studies of WNV C (Dokland *et al*., 2004). Two different buffers were used in all experiments: TEE-KCl buffer (20 mM Tris-HCl, 100 mM KCl, 1 mM EDTA and 1 mM EGTA, pH 7.4) and TEE-NaCl buffer (20 mM Tris-HCl, 100 mM NaCl, 1 mM EDTA and 1 mM EGTA, pH 7.4). Cell culture was performed with the high-glucose Dulbecco's modified Eagle's medium (DMEM) with 0.01% sodium pyruvate and 4 mM $_{L}$-glutamine, supplemented with 10% fetal bovine serum, 100 U/mL penicillin and 100 µg/ml streptomycin. Oleic acid was used at a concentration of 10 mM. To disrupt cells a cell disruption vessel model 4639, from Parr Instrument Company (Moline, IL, USA) was used. Unless otherwise stated, all other chemicals were purchased from Sigma-Aldrich (St. Louis, MO, USA).

Cell culture and lipid droplets isolation

Lipid droplets were isolated from baby hamster kidney cells (BHK-21) through a method well-established in the host laboratory (Carvalho *et al*., 2012). BHK-21 cell line was maintained in DMEM with 0.01% sodium pyruvate and 4 mM L-glutamine, supplemented fetal bovine serum, penicillin and streptomycin in a T75 culture flask. Cells were grown at 37 °C, in a humidified 5% carbon dioxide incubator. After 24 h, approximately 80% confluence was reached and the cells were treated with trypsin and divided for three T75 culture flasks. After 48 h, when approximately 80% confluence was reached in the three T75 culture flasks, each T75 culture flask was treated with trypsin and the cells were divided to ten T75 culture flasks. The thirty T75 culture flasks were maintained at 37 °C in a

humidified 5% carbon dioxide incubator. After 72 h, when approximately 80% confluence was reached in the thirty T75 culture flasks, the DMEM of each T flask was replaced for DMEM without fetal bovine serum and antibiotics, and cells were treated with 10 µM oleic acid.

Lipid droplets purification

After 24 h with oleic acid, LDs were isolated. For this, cells were washed twice and resuspended in 3 mL TEE buffer 100 mM KCl with a protease inhibitor cocktail. Following, cells were disrupted by nitrogen cavitation at 700 lb/in^2 for 20 min at 4 °C using the cell disruption vessel. The cell lysate was centrifuged at 1,500 × *g* for 10 min to remove the nuclei, and the supernatant was collected and mixed with an equal volume of TEE-KCl buffer containing 1.08 M sucrose. The sample was transferred into a 12-mL ultracentrifugation tube and sequentially overlaid with 2 mL each of 0.270 M sucrose in TEE-KCl buffer, 0.135 mM sucrose in TEE-KCl buffer, and TEE-KCl buffer without sucrose. The sample in the sucrose gradient was centrifuged at 250,000 × *g* for 70 min at 4 °C. Three fractions were collected from the top to the bottom of the gradient, faction 1 (1 mL), fraction 2 (1.5 mL) and fraction 3 (1 mL). The gradient fractions were kept at 4 °C before use. Only fraction 2 was used in the experiments, as it was previously proven to be absent of cytosolic contamination, lowest at lactate dehydrogenase (LDH) activity and enriched in one of the major LD protein components, ADRP (Carvalho *et al*., 2012). Before the use of LDs in experiments, fraction 2 collected was tested by ζ-potential measurements to determine if it present the expected and previously reported ζ-potential value (-19 mV) (Carvalho *et al*., 2012). The same protocol was performed to isolate LDs in TEE buffer 100 mM NaCl.

ζ-potential analysis of LDs surface charge

ζ-potential measurements were carried out on a Malvern Zetasizer Nano ZS (Malvern, United Kingdom) equipped with an He-Ne laser (632.8 nm). The physical constants used for the calculations were: n_0 = 1.330, η = 0.8872 cP, T = 298.15 K, λ = 632.8 nm and θ = 13º. LDs samples were equilibrated for 15 min, at 25ºC, at the Zetasizer, and then ζ-potential was determined from the average of 15 measurements (100 runs each), with 90 s of waiting between the measurements. Samples were analyzed by measuring independently the ζ-potential of LDs in a final volume of 842.5 uL after incubation for 15 min at room temperature with different concentrations of WNV C. Following previous approaches (Carvalho *et al*., 2012; Martins *et al*., 2012), limited proteolysis of LDs with trypsin was performed by incubating the LDs samples with 10 µM trypsin in TEE buffer (TEE-KCl or TEE-NaCl) for 15 min at room temperature. To stop the reaction, 1 mM phenylmethylsulfonyl fluoride (PMSF) was added to the mixture for 5 min at room temperature, after which the ζ-potential of trypsinized LDs samples was analyzed by measuring independently LDs in a final volume of 842.5 uL after incubation for 15 min at room temperature with different concentrations of WNV C protein. The variation of zeta potential (∆ζ) for each LDs sample was determined by subtracting the value of the ζ-potential of LDs in the absence of WNV C from the ζ-potential of LDs in the presence of a given WNV

C concentration. This variation in the ζ-potential of LDs can be represented as a function of WNV C concentration, fitting the experimental data with the following equation:

$$\Delta\zeta = \frac{\Delta\zeta_{max}[WNV\ C]}{C_{1/2}+[WNV\ C]} \quad \textbf{(10)}$$

where $\Delta\zeta_{max}$ is the maximum amplitude of variation of the ζ-potential induced by the interaction with WNV C and $C_{1/2}$ is the WNV C concentration at $\Delta\zeta_{max}/2$ or, in other words, is half of the protein concentration needed to saturate all the LDs in suspension.

LDs and lipoproteins preparation for force spectroscopy measurements

Ten µL of LDs suspension (fraction 2) or human plasma lipoproteins solution (VLDL and LDL) were placed onto thin freshly cleaved muscovite mica and allowed to deposit for 30 min at room temperature. Non-adherent LDs or lipoproteins were removed by 5 sequential washing steps with TEE buffer (with Na^+ or K^+, depending on the experiment). Samples were loaded into the AFM apparatus and allowed to equilibrate in the respective TEE-buffer for 10 min before force spectroscopy measurements.

Functionalization of AFM tips with WNV C

A protocol well established in the host laboratory was used to functionalize AFM tips with WNV C for force spectroscopy measurements. OMCL TR-400-type silicon nitride tips (Olympus, Japan) were cleaned with an intense UV light source and silanized in a vacuum chamber with 3-aminopropyl-triethoxysilane (APTES, 30 µL) and *N*,*N*-diisopropylethylamine (10 µL) for 1 h, under an argon atmosphere, to be coated with a self-assembled monolayer of amines. Following this, probes were rinsed with fresh chloroform and dried with nitrogen gas. The silanization process results in a uniformly distributed self-assembled monolayer of amino-terminated APTES molecules on the AFM tips, which were then placed into a 2.5% (v/v) glutaraldehyde solution for 20 min and washed 3 times with TEE buffer. Finally, the tips were placed into a 167 µM WNV C solution during 30 min to covalently bind the protein. Protein-functionalized tips were immediately mounted onto the AFM instrument and used for the force spectroscopy measurements.

AFM-based force spectroscopy measurements

Spectroscopy measurements were performed with a NanoWizard II atomic force microscope (JPK Instruments, Berlin, Germany), mounted on a top of an Axiovert 200 inverted microscope (Zeiss, Jena, Germany), using the softest triangular cantilevers with a tip radius of 15 nm and a resonance frequency of 11 kHz. The AFM head is equipped with a 15-µm z-range linearized piezoscanner and an infrared laser. First, the spring constant of the tips were calibrated by the thermal fluctuation method, resulting in values of 22 ± 5 mN/m. For each contact between LDs or lipoproteins (depending on the

experience to be conducted) and the cantilever, the distance between the cantilever and the LDs or lipoproteins was adjusted in order to maintain an applied force of 200 pN before retraction. After, molecular recognition was searched by pressing the cantilevers intermittently onto different points of LDs or lipoproteins adsorbed to the mica surface. Data were collected for each force-distance cycle at 2 µm/s, leading to a loading rate of 4 nN/s. Experiments were performed at room temperature, maintaining the laboratory between 23 °C and 25 °C. Small variations in temperature at this range did not affect the force spectroscopy measurements. In the experiments with LDs, measurements were conducted using TEE buffer (pH 7.4) with 10 or 100 mM KCl and, in order to evaluate cation dependence, 100 mM NaCl was also used in the TEE buffer instead of KCl. In the experiments with lipoproteins, measurements were conducted using TEE buffer (pH 7.4) with 100 mM KCl, both for VLDL and LDL samples, and using TEE buffer (pH 7.4) with 100 mM NaCl for VLDL samples. Each experiment was performed at least three times, each time on different samples and with different functionalized tips. For any given experiment, approximately 5,000 force-distance curves were collected, analyzed, and fitted to the worm-like-chain model (Ratto *et al*., 2006). Force curves were analyzed using the JPK image processing software v. 3 (JPK Instruments, Berlin, Germany). Histograms of the (un)binding forces of each studied protein-LD or protein-lipoprotein interaction were constructed choosing the ideal bin size to achieve the best-fitted Gaussian model peak forces. The selected binning size was 6 pN. Force rupture values ranging between 0 and 10 pN were considered to represent noise, artifacts, or nonspecific interactions. According to this, values up to 10 pN were neglected for data presentation and analysis. From each histogram, the most likely single WNV C molecule rupture force can be determined by fitting the distributions of the rupture forces with the Gaussian model. The maximum values of the Gaussian peaks represent a single-molecule-based statistical measure of the force of the molecular bond. Measurements with tips at different steps of the functionalization process (including non-functionalized tips) were conducted on glass slides, on mica, and on LDs or lipoproteins samples, which serve as controls for the AFM tip functionalization process.

DLS measurements of lipoproteins

DLS experiments were performed in the same apparatus used for the ζ-potential measurements (Malvern Zetasizer Nano ZS equipped with a He-Ne laser, λ = 632.8 nm), with a backscattering detection at 173º. For this type of measurements glass cuvettes with round aperture were used. VLDL or LDL were diluted to a final concentration of 50 µg/mL in TEE-KCl buffer and VLDL also diluted in TEE-NaCl buffer at the same final concentration. The size of booth lipoproteins was measured without WNV C. After determination of D_H value for VLDL and LDL, successive WNV C volumes were added, in order to reach concentration from 0.25 µM to 5 µM, and the D_H value was determine for each WNV C concentration. Samples were allowed to equilibrate for 15 min at 25 ºC before measurements. For every sample 10 measurements were conducted, each measurement being the average of 10 run, with 10 s of waiting between measurements. This procedure was repeated at least three times for each WNV C concentration, with independent lipoproteins samples. The normalized intensity autocorrelation functions were analyzed with the CONTIN method. The D_H

value of each measurement was obtained from the peak of the $n(D_H)$ function of each of the 10 measurements. On the experiments with pep14-23, the peptide was incubated with VLDL at 25 µg/mL, for 15 min, before measurement, and then incubated with WNV C at 5 µM before new measurements. The DLS correlograms were used to assess the details of WNV C interaction with VLDL in the presence and absence of pep14-23. Data of the lipoproteins size was statistically analyzed intra-group (of 10 measurements) by average and standard deviation, discarding outliers. The average without outliers was close to the median in all the size data points. Presented values are mean ± standard error. Data sets were compared against the first set of measurements (without WNV C) using the Mann–Whitney U test. A size data set was considered significantly different from the set without WNVC if $p < 0.05$.

III - WNV C interaction with Lipid Droplets

In this chapter it is originally demonstrated that WNV C can interact with LDs. In agreement with the data obtained for DENV, WNVC-LDs interaction may be a crucial step for viral replication and assembly. The interaction is studied in more detail, in what concerns the role of potassium ions and lipid droplets surface protein components on the interaction. The results clearly show that LDs surface proteins and potassium ions play an important role in WNV C protein interaction with LDs.

Background

There are pathogens that, upon infection, induce the accumulation of LDs in their host cells. The flaviviruses DENV (Assunção-Miranda *et al.*, 2010; Samsa *et al*., 2009) and HCV (Barba *et al.*, 1997) are known to belong to this group of pathogens and, besides promoting LDs accumulation, have their capsid protein associated with these organelles, an interaction that is essential for successful viral replication. It was shown that mutations in two L residues located in the DENV C protein hydrophobic α-helix 2 impair the protein association to LDs, suggesting the involvement of this region on the process (Samsa *et al.*, 2009). In this context, several studies were developed in the host laboratory to understand the interaction of DENV C with LDs. By the use of AFM-based force microscopy, the specific interactions between LDs and the DENV C were measured (Table 3.1) (Carvalho *et al*., 2012). It was shown that DENV C-LDs binding is dependent of potassium ions. Data from AFM-based force spectroscopy measurements with C protein-functionalized AFM tip and LDs in the presence of different potassium chlori*d*e concentrations show a typical force rupture value of 33.6 ± 0.5 pN for 100 mM KCl. That is the force necessary to break the bond between a DENV C protein dimer and a LD. A frequency of the adhesion-rupture events of 58% was determined for this process. With decreased potassium ion concentration (10 mM KCl), the percentage of (un)binding events decreased significantly and a slight increase was observed at higher concentration (400 mM KCl). When potassium ions were replaced by sodium ions in the buffer, a dramatic change is observed, with the percentage of (un)binding events and the rupture force decreasing significantly (Carvalho *et al*., 2012).

Table 3.1 - Rupture forces and percentage of (un)binding events obtained for interactions between DENV C and LDs obtained from HepG2 cell line, under diverse experimental conditions. The percentage of (un)binding events and the rupture force decrease with the reduction of potassium concentration, as well as with trypsin treatments and the replacement of potassium by sodium ions (Carvalho *et al.,* 2012).

Experimental condition	% (un)binding events	Rupture force (pN)	
		1st peak	2nd peak
Potassium ([KCl])			
10 mM	34.7	24.2	40.9
100 mM	58.4	33.6	52.4
400 mM	61.0	41.0	115.8
Trypsin pretreatment ([trypsin] in 100 mM KCl)			
1 μM	51.1	26.1	51.9
5 μM	29.4	26.6	37.7
10 μM	27.7	19.3	25.5
Sodium ([NaCl]), 100 mM	19.5	26.1	

Studies performed with ζ-potential analysis also show that potassium has a fundamental role in the DENV C-LDs interaction (Carvalho *et al*., 2012). In the absence of the C protein, LDs present a ζ-potential value of -19 mV in 100 mM KCl buffer. Higher C protein concentration induces an increase in the ζ-potential, up to 13.7 mV at the highest concentration tested (6 μM) (Figure 3.1.A). Mirroring

the AFM data, the effect of potassium is also clear, as seen from the values of $C_{1/2}$ in the presence of this ion (Figure 3.1.B).

A

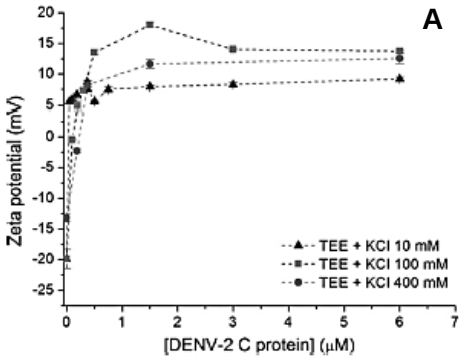

B

[KCl] (mM)	Mean $C_{1/2}$ (nM) ± SE	Mean $\Delta\zeta_{max}$ (mV) ± SE
10	5.9 ± 2.2	27.9 ± 0.4
100	85.7 ± 17.6	34.4 ± 1.3
400	188.4 ± 68.8	27.6 ± 2.3

Figure 3.1 - LDs zeta potential analysis with DENV C protein. (A) LDs zeta potential values determined in the absence and in the presence of distinct DENV C concentrations, at different KCl concentrations. (B) Values of the maximum amplitude of variation of the LDs zeta potential ($\Delta\zeta_{max}$) induced by the interaction with the DENV C protein and DENV C protein concentration at $\Delta\zeta_{max}/2$ ($C_{1/2}$) in TEE buffer with different potassium concentrations (Carvalho *et al.,* 2012).

Moreover, it is known that DENV C interacts specifically with proteins in the surface of LDs (Carvalho *et al*., 2012). When LDs are preincubated with trypsin (which is subsequently washed) the percentage of rupture force (un)binding events determined by AFM-based force spectroscopy decreased significantly compared to the experiments without preincubation with trypsin. In fact, it was demonstrated that all stronger binding events tended to disappear with the increase of trypsin concentrations, occurring only weaker interactions (Table 3.1).

As such, taking into consideration that DENV C-LD interaction is strong and specific, requiring LDs surface proteins for the binding as well intracellular potassium (Carvalho *et al*., 2012) and that the residues within the hydrophobic α2–α2' core involved in LDs interaction are conserved among flaviviruses, both in terms of sequence and structural alignment (Martins *et al*., 2012), it is likely that the same is observed for WNV C protein interaction with lipid systems. With this in mind, the WNV C protein interaction with LDs was originally tested here, by employing ζ-potential measurements and AFM-based force spectroscopy, to characterize the strength and level of specificity of the interaction.

Results

Assessment of WNV C protein-LDs interaction by ζ-potential analysis

ζ-potential measurements were performed to first test the quality of the different LDs fractions resulting from ultracentrifugation. Fraction 2 was selected as the most appropriate (in line with previous studies). 42.5 µL of LDs from this fraction were collected, and added to 800 µL TEE-KCl buffer with 100 mM KCl, presenting ζ-potential values of roughly -20 mV. These ζ-potential values were identical to the observed for LDs isolated in previous studies (discussed in the background).

WNV C-LDs interaction requires LDs surface proteins

ζ-potential measurements were performed to understand if WNV C protein is able to interact with LDs. Upon the addition of WNV C protein to LDs in K^+ buffer, there was a concentration-dependent increase in the ∆ζ-potential (Figure 3.2.A - filled symbols). In the absence of WNV C, LDs in K^+ buffer present a negative ζ- potential value (-20.6 ± 0.7 mV). The addition of WNV C to LDs suspension induced a progressive increase in the scattering particle charge (ζ-potential values increase), stabilizing at positive values (15.8 ± 0.7 mV) (Supplementary figure 2.A of annexes - filled symbols). This data suggest that WNV C can interact with LDs, as expected. With identical addition of WNV C protein to the trypsinized LDs, there was an increase in the ∆ζ-potential values (Figure 3.2.A - empty symbols). LDs have an initial value of -18.8 ± 1.2 mV that increase and stabilize at 1.5 ± 1.7 mV (Supplementary figure 2.A of annexes - empty symbols). The increase in ∆ζ-potential of non-trypsinized LDs is much higher than the increase observed for trypsinized LDs. With the same concentration of WNV C, the scattered light is higher for non-trypsinized LDs.

WNV C-LDs interaction is dependent on potassium ions

To confirm if WNV C-LD interaction is dependent of potassium ions, the LDs ζ-potential was measured replacing the TEE-KCl buffer by TEE-NaCl 100 mM (Na^+ buffer). As with the LDs in K^+ buffer, LDs in Na^+ buffer have a ζ-potential increase with the addition of WNV C protein (Figure 3.2.B - filled symbols). In this case LDs have an initial ζ-potential of -16.5 ± 0.5 mV and in the presence of WNV C increasing concentrations that value became positive (12.7 ± 0.3 mV) (Supplementary figure 2.A - filled symbols). Addition of WNV C to trypsinized LDs in Na^+ buffer result in a lower increase of LDs ζ-potential (Figure 3.2.B - empty symbols), from -16.6 ± 0.6 mV (without WNV C) up to -2.8 ± 2.3 mV (at the highest concentration of WNV C measured) (Supplementary figure 2.B - empty symbols).

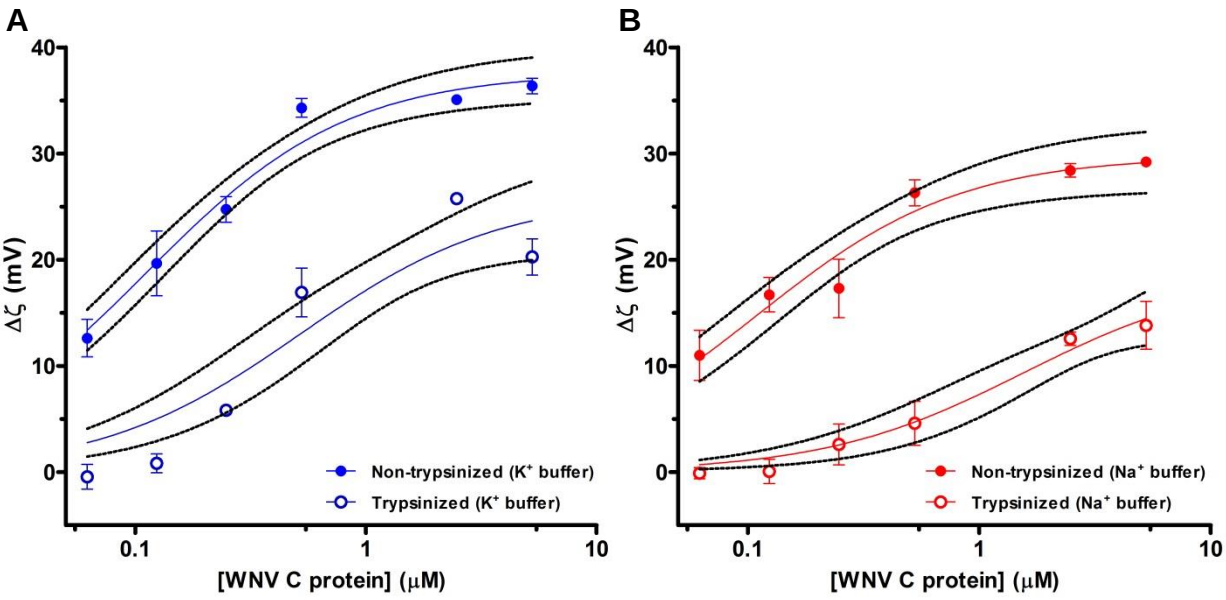

Figure 3.2 - LDs ζ-potential analysis at different WNV C concentrations. Variation of zeta potential (Δζ) values of LDs samples isolated with (A) TEE-KCl buffer (K^+ buffer) and (B) TEE-NaCl buffer (Na^+ buffer) in the absence and in the presence of distinct WNV C concentrations. ζ-potential values were determined for LDs without trypsin preincubation (filled symbols) and LDs preincubated with trypsin (empty symbols). Results are represented as mean ± standard error. Solid lines were obtained through the fitting of experimental data with equation 10. Concentrations are presented in logarithmic scale.

The fitting of the experimental data to the curve defined with equation 10 of the material and methods yield good R^2 values (Table 3.2). The values of the maximum amplitude of variation of ζ-potential induced by the interaction with WNV C ($\Delta\zeta_{max}$) and the WNV C protein concentration at $\Delta\zeta_{max}/2$ ($C_{1/2}$) are also presented on Table 3.2. Fitted curves obtained for each experimental condition are shown in Figure 3.2. For non-trypsinized LDs in K^+ buffer, a $C_{1/2}$ of 112 ± 15.3 nM was obtained. In the case of trypsinized LDs, a $C_{1/2}$ value 4.6-fold higher (519 ± 168 nM) is obtained, showing that LDs surface proteins are an essential part of the interaction. When K^+ buffer was replaced by Na^+ buffer, a $C_{1/2}$ of 111 ± 21.3 nM for non-trypsinized LDs and 1560 ± 697 nM to trypsinized LDs (14-fold higher) were observed.

Table 3.2 - Parameters obtained by ζ-potential analysis of LDs under different conditions. The values of $C_{1/2}$ and $\Delta\zeta_{max}$ were obtained through the fitting of ζ-potential experimental data with equation 10.

Condition		Mean $C_{1/2}$ ± S.E. (nM)	Mean $\Delta\zeta_{max}$ ± S.E. (mV)	R^2
K^+ buffer	Non-trypsinized	112 ± 15.3	37.6 ± 1.16	0.93
	Trypsinized	519 ± 168	26.0 ± 2.45	0.84
Na^+ buffer	Non-trypsinized	111 ± 21.3	29.8 ± 1.51	0.90
	Trypsinized	1560 ± 697	18.8 ±3.07	0.86

* Shown are values of the maximum amplitude of variation of the LDs zeta potential ($\Delta\zeta_{max}$) induced by the interaction with WNV C, and the WNV C concentration at $\Delta\zeta_{max}/2$ ($C_{1/2}$), in K^+ and Na^+ buffers, with non-trypsinized LDs and trypsinized LDs.

Assessment of WNV C-LDs interaction by AFM-based force spectroscopy

Binding force measurements and potassium ion dependence

By AFM-based force spectroscopy, it was possible to measure specific interactions between LDs and WNV C from the adhesion profiles obtained for each force curve. WNV C-LDs (un)binding forces were measured based on the deflection of AFM tips functionalized with WNV C upon interacting with LDs. Comparing the rupture length histograms of functionalized and non-functionalized AFM tips showed a partial overlay of both histograms at rupture lengths above 50 nm (data not shown). With the movement of the AFM tip, some LDs occasionally adhere to the tip and detach from the mica, resulting in (un)binding events between the LDs attached to the tip and those on the mica surface. To ensure that only the direct interactions between the C protein on the tip and LDs that are firmly adherent on mica are considered, only the force-distance events that occurred at a rupture length below 50 nm were taken into consideration. Thus, any interference from events resulting from LDs-LDs interactions was excluded.

Figure 3.3 shows the force rupture histogram obtained for the normalized frequency of the forces of the (un)binding events between the C protein-functionalized AFM tip and LDs in the presence of different potassium chloride concentrations. The distribution of the length of the rupture adhesion events between WNV C and LDs was analyzed by fitting the obtained histogram with the Gaussian model described previously in material and methods. A force rupture value of 30.38 ± 0.33 pN was obtained for 100 mM KCl (Figure 3.3.A). This value corresponds to the force necessary to break the bond between a WNV C protein dimer and a LD. The peak with weaker interaction forces (17.67 ± 47.1 pN) corresponds to unspecific interactions. The two other peaks of stronger interaction forces (52.04 ± 2.49 pN and 108.52 ± 2.82 pN) correspond to the rupture of multiple bonds due to the interaction of more than one protein dimer attached to the tip with a LD.

Force spectroscopy measurements were also performed decreasing the potassium concentration in the buffer from 100 mM to 10 mM, to evaluate the types of force involved in the binding between WNV C and LDs (Figure 3.3.B). The decrease of the potassium concentration of the buffer causes a significant decrease in the percentage of (un)binding events, from 62.7% in TEE buffer with 100 mM KCl to 19.4% in TEE buffer with 10 mM KCl (Table 3.3). At a low potassium concentration, the force histogram changes significantly. Only two force peaks were observed for TEE buffer with 10 mM KCl. The first peak with 20.05 ± 0.19 pN and the second peak with 29.59 ± 0.89 pN. However, the second peak is similar to that observed for TEE buffer with 100 mM KCl (30.38 ± 0.33 pN), corresponding to the force necessary to break the bond between a WNV C dimer and a LD. Interaction forces corresponding to the rupture of multiple bonds, due to the interaction of more than one protein dimer attached to the tip with a LD, were not observed at low potassium concentration.

.

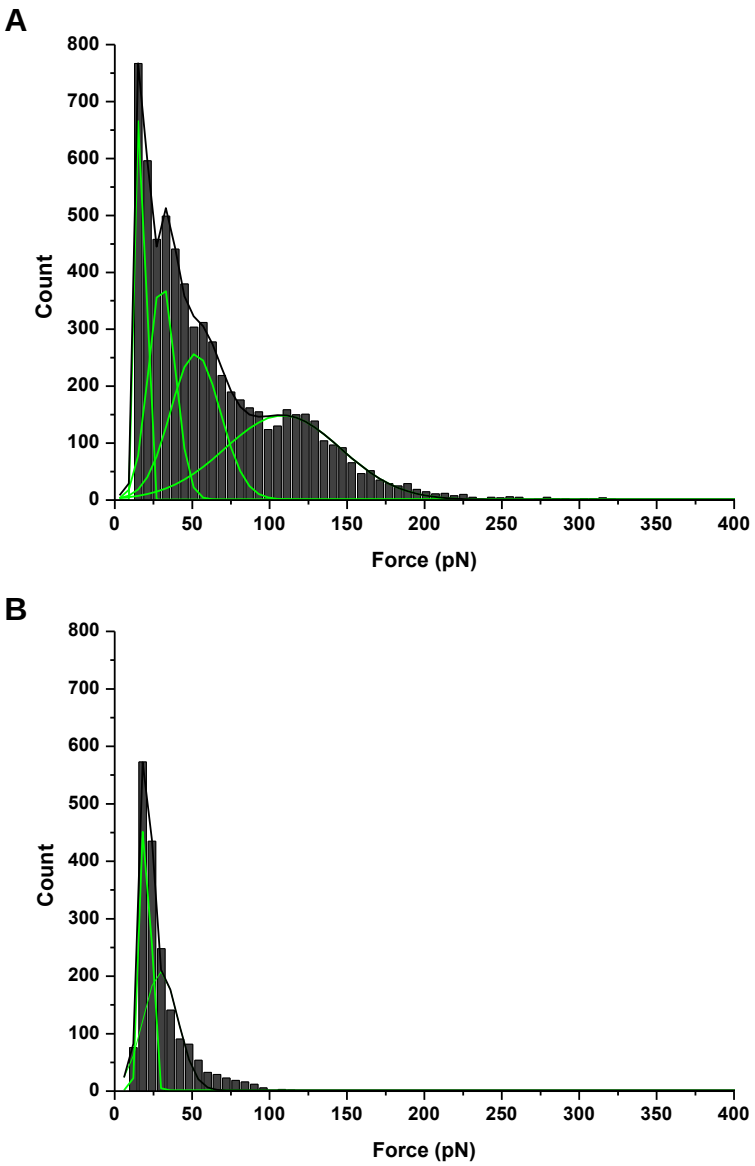

Figure 3.3 - Force rupture histograms of the binding of WNV C to BHK-21 LDs in TEE buffer with (A) 100 mM KCl and (B) 10 mM KCl. Four peaks of rupture forces were observed for TEE buffer with 100 mM KCl (1: 17.67 ± 47.81 pN; 2: 30.38 ± 0.33 pN; 3: 52.04 ± 2.49 pN; 4: 108.52 ± 2.82 pN) and two peaks for TEE buffer with 10 mM KCl (1: 20.05 ± 0.19 pN; 2: 29.59 ± 0.89 pN).

Effect of sodium ions on WNV C-LDs interaction

When force spectroscopy measurements were performed with potassium replaced by sodium (Figure 3.4), a dramatic change in the results was observed. Applying the Gaussian model to the histogram profile obtained, a single peak of rupture force at 17.88 ± 0.14 pN was observed. A significant decrease in the percentage of (un)binding events from 62.7% in TEE buffer with 100 mM KCl to 19.3% TEE buffer with 100 mM NaCl is also observed (Table 3.3). This means that the probability of occurrence of strong (un)binding events decreases, leaving only the weaker (un)binding events characteristic of unspecific interactions. WNV C-LDs interaction is therefore K^+ specific rather than a general effect of the ionic strength.

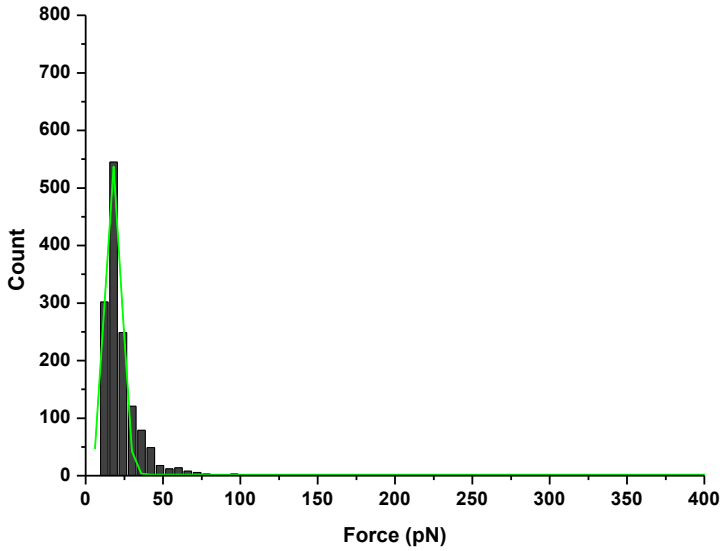

Figure 3.4 - Force rupture histogram of the binding of WNV C to BHK-21 LDs in TEE buffer with 100 mM NaCl. One peak of rupture force at 17.88 ± 0.14 pN was observed between WNV C and LDs in TEE buffer with 100 mM NaCl.

Table 3.3 - Rupture forces and percentage of (un)binding events observed with AFM-based force spectroscopy for the interaction between WNV C and BKH-21 LDs at different experimental conditions.

Experimental Conditions	(un)binding events (%)	Rupture Force (pN)			
		1st peak	2nd peak	3rd peak	4th peak
Potassium [KCl]					
100 mM	62.7	17.67	30.38	52.04	108.52
10 mM	19.4	20.05	29.59		
Sodium [NaCl]					
100 mM	19.3	17.88			

Discussion

The ζ-potential measurements of LDs at pH 7.4 and 100 mM KCl revealed a negative surface charge, with an average of -20.6 ± 0.7 mV. This negative charge was observed in previous studies with LDs isolated by the same procedure (Carvalho *et al*., 2012). In fact, a negative charge was expectable, due to the phospholipid monolayer at the LDs surface containing anionic phospholipids. After interaction with WNV C, the LDs negative surface charge becomes positive, reaching a maximum plateau at 15.8 ± 0.7 mV. These results are in agreement with the data collected for DENV C: LDs ζ-potential of -19 mV in the absence of DENV C and 13.7 in the presence of DENV C (6μM). The interaction between DENV C and LDs was shown to be essential, in different cells types, for the viral replication cycle (Samsa *et al.*, 2009). Single DENV C-LD interactions were found to be strong and characteristic of specific binding, with a (un)binding force of 33.6 ± 0.5 pN (Carvalho *et al*., 2012), which is of the same order of magnitude of several specific protein-protein, protein-ligand and protein-phospholipid bilayer interactions previously studied by force spectroscopy (Desmeules *et al.*, 2010). In the present study, we performed AFM-based force measurements to understand the WNV C-LDs interaction at the single-molecule level. As for DENV C, we found that single WNV C-LD interactions are strong and characteristic of specific binding, with a (un)binding force of 30.38 ± 0.33 pN.

On our ζ-potential experiments with trypsinized LDs, an initial ζ-potential of -18.8 ± 1.2 mV was observed. After the addition of WNV C, this negative surface charge becomes positive, reaching a maximum of 1.5 ± 1.7 mV. Considering that the treatment with trypsin affects the proteins at the surface of LDs and that upon the addition of the C protein their surface charge increment is much lower, we can hypothesize that WNV C interaction with LDs requires proteins in their surface. Fitting the ζ-potential values obtained for non-trypsinized LDs with equation 10, we observed a maximum variation in the ζ-potential of 37.6 ± 1.16 mV and a $C_{1/2}$ of 112 ± 15.3 nM, in concordance with the values obtained for DENV C ($\Delta\zeta_{max}$ of 34.4 nM and $C_{1/2}$ of 87.7 nM) in previous studies (Carvalho *et al*., 2012). LDs contain several proteins on their surface, majorly the proteins of PAT family, namely, perilipin (perilipin 1), ADRP (perilipin 2), TIP47 (perilipin 3), and other proteins in minor quantities (Olofsson *et al.*, 2009). As discussed before in the background, it was found that DENV C interacts with LDs through a protein-protein interaction and not a protein-lipid interaction. In fact, it was found that TIP47 probably is the protein involved in this interaction (Carvalho *et al.*, 2012). The variation in the ζ-potential observed upon titration with DENV C or WNV C is identical, reinforcing the idea that the proteins are very similar and interact with LDs in the same way. Moreover, $C_{1/2}$ is also in the same order. For trypsinized LDs, upon addition of WNV C, we observed a higher $C_{1/2}$ of 519 ± 168 nM and the variation in the ζ-potential is much lower ($\Delta\zeta_{max}$ of 26 ± 2.45 mV), in agreement with the hypothesized before for WNV C interaction with proteins in the LDs surface.

ζ-potential analysis was also used to probe the influence of cations in the binding between WNV C and LDs. LDs isolated in sodium buffer present a ζ-potential slightly different from the observed for LDs isolated in potassium buffer. In the absence of C protein, LDs have an average ζ-potential of -16.5 ± 0.5 mV that increases to 12.7 ± 0.3 mV upon interaction with the protein. In this case a $C_{1/2}$ of 111 ± 21.3 nM was observed. This value is identical to the determined in potassium

buffer; however, the $\Delta\zeta_{max}$ in sodium buffer is significantly different (29.8 ± 2.45 mV). These findings suggest that the interaction between WNV C and LDs may be K^+-dependent. The force spectroscopy approach was also used to probe the influence of sodium ion in the binding between WNV C and LDs. A marked decrease in both the percentage of events and the (un)binding force were observed: 19.3 % and 18.88 pN, respectively. The replacement of potassium by sodium (a monovalent cation of lower size) decreased significantly the binding between WNV C and LDs, demonstrating that the interaction is K^+-dependent and that the decreased binding observed at low potassium concentration is not a consequence of the decreased ionic strength, but of a decrease of the potassium concentration itself. These findings are in agreement with the results observed by ζ-potential analysis. Considering that K^+ is the main intracellular cation, when its concentration is low in the extracellular medium, where Na^+ is the main cation, it is possible that the K^+-dependent interactions between WNV C (and the C proteins of other *Flavivirus*) and LDs may be involved in the WNV C protein release in the cytosol. Other viruses requires require K^+ for their infection processes. It was found that HCV modulates the function of a K^+-specific channel (Kv2.1) with the viral nonstructural protein NS5A (Mankouri *et al.*, 2009). HCV also utilizes a viroporin (viral proteins that enhance cell membrane permeability in order to favor viral replication), p7, to promote membrane permeability to potassium and other cations in their infection process (Griffin *et al.*, 2003). In fact, when viruses invade the host cells, the infectious process modulates their biochemistry and physiology. These mechanisms are frequently essential for the viral life cycle (Wang *et al.*, 2011). It is expected that WNV C interaction with LDs is essential for replication, as mentioned for other *Flavivurus*, such as HCV and DENV (McLauchlan, 2009).

In order to evaluate if WNV C can interact with LDs in the absence of potassium ions or after limited proteolysis of LDs, ζ-potential analysis were performed with LDs isolated in sodium buffer or submitted to a pre-treatment with trypsin. Those LDs presented an initial ζ-potential (-16.6 ± 0.6 mV) equal to LDs isolated in sodium buffer non-trypsinized, which upon titration with WNV C increase to -2.8 ± 2.3 mV. Dramatic changes on $C_{1/2}$ and $\Delta\zeta_{max}$ were observed. The half of the protein concentration needed to saturate LDs in suspension increased to 1560 ± 697 nM and a maximum variation in ζ-potential of 18.8 ± 3.07 mV was determined. These values show that in the absence of potassium ions or after limited proteolysis of LDs, WNV C-LDs binding decrease significantly. Based on our finding, we can propose that WNV C binds to protein(s) on the surface of intracellular LDs and the interaction is not electrostatic-driven, but depends on the intracellular high potassium concentration. It is expected that *Flavivirus* C proteins interact specifically with proteins on the LDs surface through a mechanism dependent on potassium concentrations. Furthermore, the function of C proteins can be conserved among *Flavivirus* and be essential for the replication process.

IV - WNV C interaction with Lipoproteins

Flaviviridae family members, such as HCV and DENV, are able to fuse with very low-density lipoproteins (VLDL) to form lipoviroparticles (LVPs), as a key step of the infection process. This chapter is focused on the ability of WNV C to interact with human lipoproteins, namely VLDL and LDL. The results show, for the first time, that WNV C can interact with VLDL (but not with LDL) in a potassium ion-dependent manner that closely resembles DENV C interaction with lipoproteins and which may lead the formation of highly infectious LVPs in WNV infection.

Background

DENV C, homologous of WNV C, is able to interact with VLDL (Faustino *et al*., 2014). This interaction is specific and dependent on potassium ions. The (un)binding forces between DENV C and VLDL were determined via AFM-based force spectroscopy. In contrast to VLDL, DENV C cannot interact with LDL. Moreover, when potassium ions from the buffer are substituted by sodium ions at the same concentration, the force histogram generated from the interaction between DENV C and VLDL only shows the weaker unspecific forces peak. Supporting AFM data, DLS measurement indicate that DENV C can interact with VLDL but not with LDL (Faustino *et al*., 2014). DLS studies of DENV C-VLDL and DENV C-LDL binding show that in the absence of DENV C, LDL and VLDL present average hydrodynamic diameters (D_H) of 23.5 ± 0.43 nm and 35.4 ± 0.55 nm, respectively. When titrated with DENV C, VLDL increase their D_H by ~6 nm, in contrast to LDL, for which no significant differences were observed (Figure 4.1) (Faustino *et al.*, 2014). These data supports a model where the DENV C dimer binds to the VLDL surface, forming a single viral protein monolayer. It was proposed that, as HCV (Bartenschlager *et al.*, 2011), DENV C can interact with VLDL and form LVPs (Faustino *et al*., 2014).

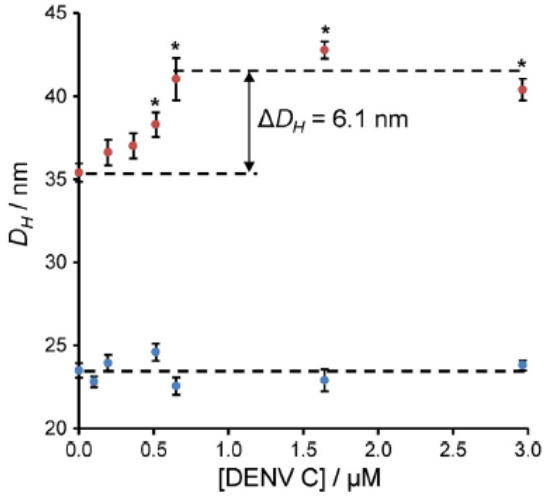

Figure 4.1 - Lipoproteins average diameter evolution upon titration with DENV C determined by DLS. DENV C interacts with VLDL (red) and forms a conjugate with a D_H ~6 nm higher than in the absence of DENV C (*p < 0.005). LDL (blue) do not form the same type of conjugate (no statistically significant variations on D_H, p > 0.05), indicating that DENV C does not interact with LDL (Faustino *et al.*, 2014).

Local structural changes involving specific conserved amino acid residues localized in the disordered N-terminal region in the central hydrophobic patch and in the loop between α1 and α2 were identified, which enabled attribute to the N-terminal disordered region of the C protein a new function (Martins *et al*., 2012). With this information, a peptide (pep14-23) was designed based on the residues 14 to 23 of the N-terminal domain of DENV C (only Glu^{19} was replaced by an alanine to make the sequence more similar to the C protein of all *Flavivirus*). pep14-23 is a short peptide that begins in the first residue of the conserved motif and extends to the last residue affected by LDs interactions, which includes the conserved motif NML+R. This peptide demonstrated to be able to interact specifically with

LDs, and compete with DENV C for its LDs-binding, consequently inhibiting the DENV C-LDs interaction (Martins *et al*., 2012). Furthermore, in subsequently studies to test if pep14-23 is able to inhibit DENV C-VLDL interaction, it was demonstrated that pep14-23 successfully inhibit this binding, a process important for the formation of LVPs and viral infection (Faustino *et al*., 2014). DLS and AFM-based force spectroscopy experiments with VLDL and DENV C in the presence of pep14-23 show an inhibition of the DENV C-VLDL interaction (Faustino *et al*., 2014). DLS experiments demonstrated that DENV C forms aggregates with VLDL, but when VLDL were previously incubated with pep14-23 the system does not aggregate in a so larger extent, suggesting that pep14-23 inhibit the interaction of DENV C with VLDL. According to these results, the AFM-based force spectroscopy measurements of the interaction between DENV C and VLDL in the presence of increasing pep14-23 concentrations show a significant decrease on the percentage of (un)binding events (Faustino *et al*., 2014). It was also shown that pep14-23 can interact with negatively charged lipids and acquire an α-helical conformation on membrane environments. Furthermore, it was demonstrated that this conversion to α-helical conformation is independent of K^+ ions. Since this peptide was designed based on a conserved region of the N-terminal of *Flavivirus* C proteins, it is expectable that it may also inhibit the interaction of WNV C with the same lipid systems.

Considering all this information, in the present chapter the ability of WNV C to interact with human lipoproteins isolated from human blood was studied employing DLS and AFM-based force spectroscopy methodologies. The results obtained suggest that WNV C can interact with VLDL, but not with LDL, in a potassium dependent manner. To evaluate the hypothesis that pep14-23 can inhibit this interaction between WNV C and VLDL, DLS measurements were performed to understand if in the presence of pep14-23 and WNV C in suspension, the average size of VLDL is affected by the interaction with WNV C.

Results

Assessment of WNV C-VLDL interaction by dynamic light scattering

VLDL apparent size increase in the presence of WNV C

By DLS, it was possible to measure the scattered light intensity fluctuations of lipoproteins that occur due to their Brownian motion, and calculate using the Stokes-Einstein equation their hydrodynamic diameter (D_H). Measuring the average particle size of lipoproteins with this technique, an increase in the VLDL size upon titration with WNV C was observed (Figure 4.2 - blue). DLS data shows that in the absence of WNV C, VLDL and LDL presents an average size of 38.2 ± 0.7 nm and 22.1 ± 0.4 nm, respectively, which are in concordance with the literature. Upon the titration with increasing concentrations of WNV C, there was a statically significant increase in the average size of VLDL to 42.8 ± 0.5 nm ($p < 0.005$). The VLDL D_H in the presence of WNV C has a 4.5 ± 0.6 nm increase relative to the value in the absence of the protein. By the observation of $I(D_H)$ distribution of the measurements, it is possible to say that these values do not correspond to aggregation that may occur in a small fraction of the total particles, but to an increase in the average size of VLDL due to the interaction with WNV C. In the case of LDL, upon titration with WNV C there was no increase in the average size (Figure 4.2 - green). Only with higher concentration of WNV C an increase in the size of LDL statistically different from the initial value occurs ($p < 0.005$).

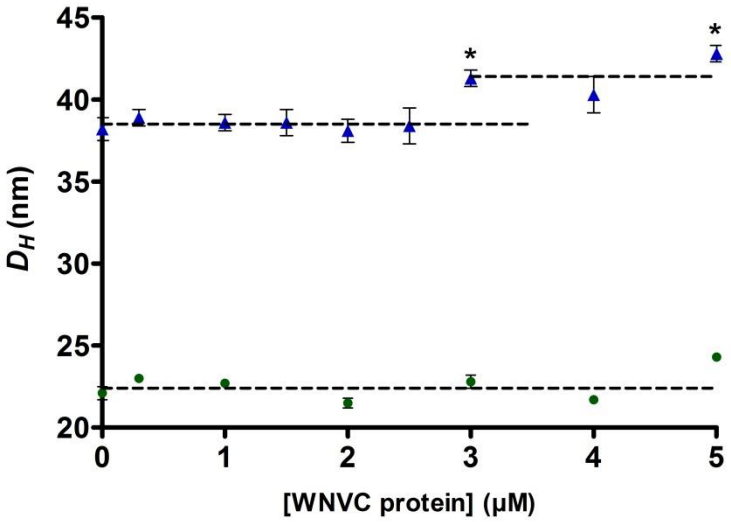

Figure 4.2 - DLS analysis of lipoproteins in potassium buffer. Lipoproteins hydrodynamic diameters (D_H) were determined in the absence and in the presence of increasing WNV C concentrations. VLDL (blue) average hydrodynamic diameter increases in the presence of WNV C, ΔD_H = 4.5 ± 0.6 nm. The D_H of LDL (green) in the absence and presence of WNV C do not change significantly, only with higher concentration of WNV C (5 μM) a statistically significant variation ($p < 0.005$) occurs. The values represented are the average of all measurements for each point (error bars represent standard error and dashed lines the average of each set of points).

WNV C-VLDL interaction is dependent on potassium ions

In order to test if potassium ions have an important role in the WNV C-VLDL interaction, the size of VLDL was measured replacing TEE-KCl buffer by TEE-NaCl (Figure 4.3). VLDL in TEE-NaCl buffer have a higher D_H initial value (40.5 ± 0.6 nm). Upon titration with WNV C, there is not a significant difference in D_H. These results suggest that in the absence of potassium ions WNV C cannot interact with VLDL, supporting that K^+ seems to be crucial for WNV C-VLDL interaction.

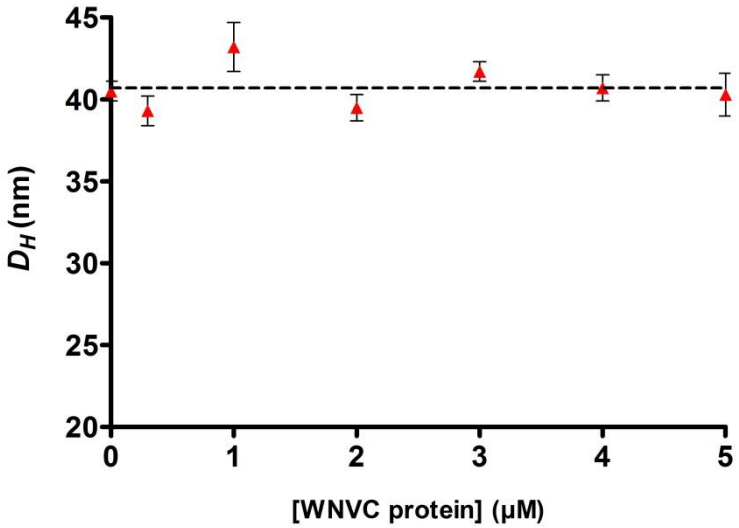

Figure 4.3 - DLS analysis of VLDL in sodium buffer. VLDL hydrodynamic diameters (D_H) were determined in the absence and in the presence of increasing WNV C concentrations in TEE NaCl 100 mM buffer. The D_H of VLDL in the absence and presence of WNV C do not change significantly. The values represented are the average of all measurements for each point. Error bars represent standard error and the dashed line the average of all points.

VLDL size increment correlates with WNV C dimensions

Based on DLS data, we could deduce a model for WNV C-VLDL interaction, where WNV C dimer binds to the VLDL surface, forming a single viral protein layer (Figure 4.4). VLDL have a hydrodynamic radius of approximately 19 nm. When WNV C interacts with its surface, the radius increases to approximately 21.3 nm. This 2.3 nm increment correlates with the dimension of the WNV C dimer.

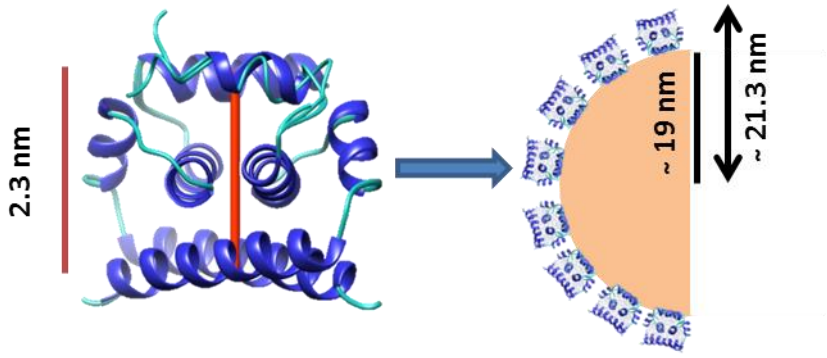

Figure 4.4 - Model for the interaction of WNV C with VLDL. The dimensions of WNV C fit well with the observed increase of ~4.5 nm on the VLDL hydrodynamic diameter (~2.3 nm for the radius), determined by DLS. In the absence of WNV C, VLDL presented a radius of ~19 nm. In the presence of WNV C 5 µM, VLDL presented a radius of ~21.3 nm. WNV C seems to bind to the VLDL surface in a sufficient number to cause a significant increase on their size, forming a protein monolayer. This monolayer does not have to be continuous.

Assessment of WNV C-VLDL interaction by AFM-based force spectroscopy

With AFM-based force spectroscopy it was possible to confirm and characterize the WNV C interaction with VLDL. The same approach used to characterize the WNV C-LDs interaction was employed to measure the parameters of WNV C binding to human plasma lipoproteins (VLDL and LDL). In the same order, through the deflections of the AFM tip functionalized with WNV C, the (un)binding forces between VLDL or LDL and WNV C were measured. To exclude interferences resulting from non-specific interactions (interactions that also appeared in the controls performed with non-functionalized tips and lipoproteins), forces below 30 pN were considered as unspecific. The distribution of the length of the rupture adhesion events between WNV C and VLDL or LDL were analyzed by fitting the obtained histograms with the Gaussian model. Figure 4.5 presents the histograms of WNV C interaction with VLDL and with LDL, both in the presence of TEE buffer with 100 mM KCl. Comparing the histograms for VLDL and LDL, different peaks, corresponding to different rupture forces, can be seen. In the VLDL histogram (Figure 4.5.A), beside the unspecific interactions (20.96 ± 0.29 pN), strong and specific interactions were observed (82.88 ± 0.65 pN). The LDL histogram (Figure 4.5.B) shows only weak forces (24.53 ± 0.09 pN), characteristic of unspecific interactions. Moreover, the percentage of (un)binding events registered for VLDL (31.1%) is much higher than for LDL (3.1%) (Table 4.1).

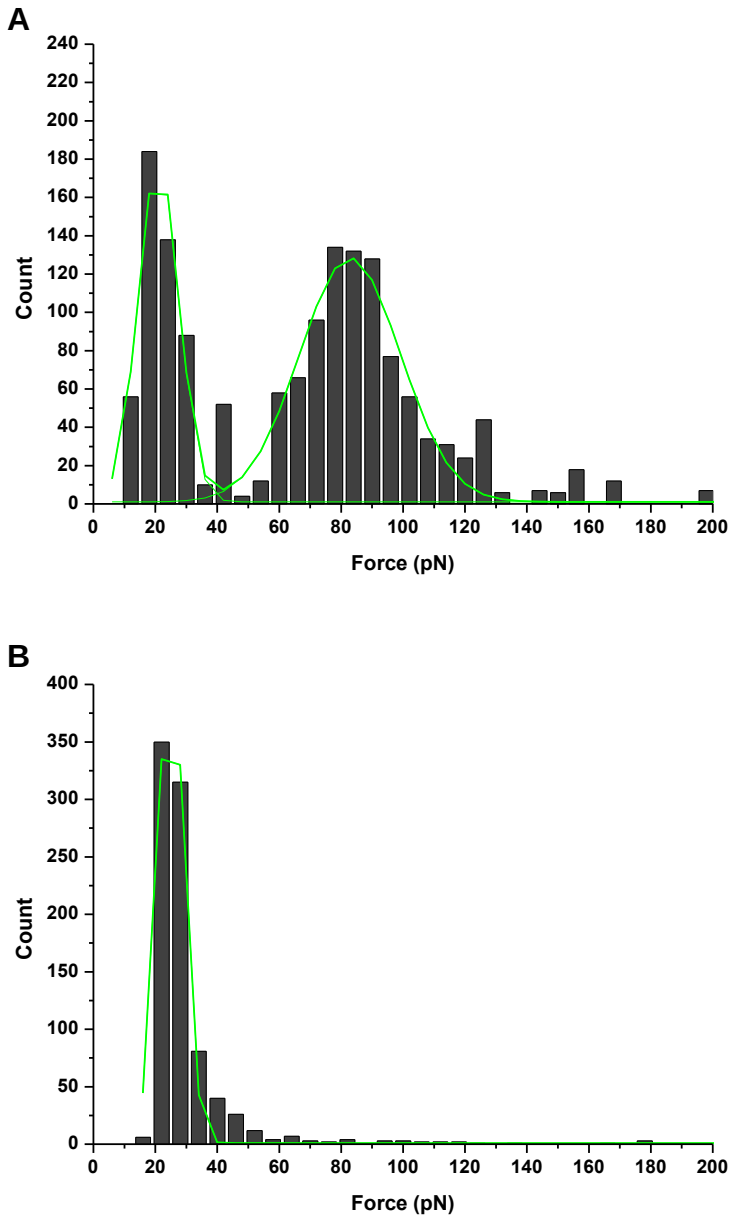

Figure 4.5 - Force rupture histograms of WNV C interactions with (A) VLDL or (B) LDL, in TEE buffer with 100 mM KCl. Two rupture force peaks were observed for VLDL (1: 20.96 ± 0.29 pN; 2: 82.88 ± 0.65 pN) and one for LDL (24.53 ± 0.09 pN).

In order to determine if these binding events between WNVC and VLDL are dependent from potassium ions, the interactions were also measured in the presence of TEE buffer with 100 mM NaCl (Figure 4.6). Interestingly, the strong and specific interactions that occur in TEE buffer 100 mM KCl disappear when the ionic strength is maintained but potassium ions are replaced for sodium ions. In the histogram, only a peak of weak forces is observed (24.96 ± 0.08 pN), corresponding to unspecific interactions. In agreement with these results, the percentage of (un)binding events also decreases significantly to 15.1% (Table 4.1). Therefore, WNVC-VLDL interaction seems to be potassium dependent.

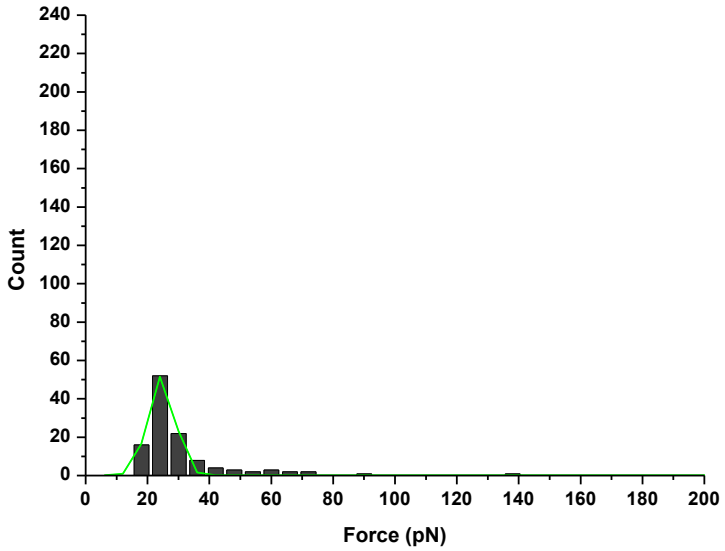

Figure 4.6 - Force rupture histogram of WNV C interaction with VLDL in TEE buffer with 100 mM NaCl. Only one rupture force peak is observed (24.96 ± 0.08 pN).

Table 4.1 - Rupture forces and percentage of (un)binding events determined with AFM-based force spectroscopy for the interaction between WNV C and VLDL or LDL at different experimental conditions.

Experimental Conditions	(Un)binding Events (%)	Rupture Forces (pN)	
		1st peak	2nd peak
Potassium [KCl] 100 mM			
VLDL	31.1	20.96	82.88
LDL	3.1	24.53	
Sodium [NaCl] 100 mM			
VLDL	15.1	24.96	

pep14-23, a possible inhibitor of WNVC-VLDL interaction

By performing DLS experiments with VLDL and WNV C in the presence of pep14-23 an inhibition of the WNV C-VLDL interaction is visible (Figure 4.7). In the DLS experiments, VLDL in suspension in TEE buffer with 100 mM KCl have a decay on the intensity autocorrelation function characteristic of VLDL that is highly reproducible (Figure 4.7 - blue line). When the experiments with VLDL were performed in the presence of WNV C, a delay in the decay of the intensity autocorrelation function becomes clear (Figure 4.7- black line). VLDL in the presence of WNV C form complexes that lead to a slower decrease in the autocorrelation function. These data are in agreement with the results previously shown in Figure 4.2. The slower decrease in the function is due to the WNV C-VLDL binding, and not to other types of aggregation, which may be occurring but at a lower proportion. VLDL

in the presence of pep14-23 100 µM (Figure 4.7- red line) does not form the same complexes, as the autocorrelation function superimposes well with the correlogram of VLDL alone. When VLDL were preincubated for 15 min with pep14-23 (100 µM) in the presence of WNV C (5 µM) (Figure 4.7- green line), the decay in the autocorrelation function is different from the previously observed. In this case, complexes are formed, although the decrease in the light scattering autocorrelation function is faster than for VLDL in the presence of WNV C without pep14-23. As the VLDL-protein complexes are not formed in such a larger extent, this indicates that pep14-23 may be inhibiting the interaction of WNV C with VLDL.

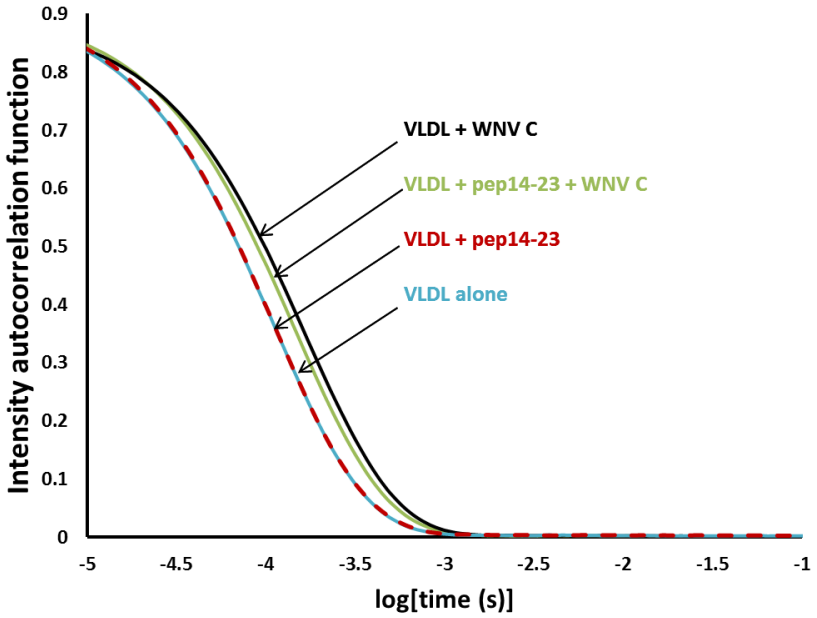

Figure 4.7 - DLS correlograms of VLDL measured in different conditions: blue line – VLDL alone; red line – VLDL incubated with pep14-23 100 µM; green line – VLDL preincubated with pep14-23 100 µM and after with WNV C 5 µM; black line – VLDL and WNV C.

Discussion

WNV C-VLDL interaction was demonstrated via DLS spectroscopy, monitoring the particle size. In the absence of WNV C, LDL and VLDL presented an average hydrodynamic diameter (D_H) of 22.1 ± 0.4 nm and 38.2 ± 0.7 nm, respectively. These values are consistent with those reported in the literature (Cushley and Okon, 2002). Upon the addition of WNV C, a complex with VLDL is formed, leading to an increase in diameter by 4.5 ± 0.6 nm. In contrast, no significant change was observed in the LDL size, suggesting that WNV C only interacts with VLDL, as previously reported for DENV C (Faustino *et al*., 2014). Furthermore, via DLS spectroscopy it was possible to evaluate if WNV C protein-VLDL interaction is dependent of potassium ions. As for ζ-potential analysis to evaluate the interaction of WNV C with LDs, the potassium buffer was replaced for sodium buffer in the DLS measurements. Interestingly, the initial average hydrodynamic diameter of VLDL in sodium buffer (40.5 ± 0.6 nm) is higher than for VLDL in potassium. Upon titration of VLDL in sodium buffer with WNV C, the average D_H did not change significantly. These finds suggest that WNV C-VLDL interaction requires potassium ions. Supporting these results, AFM-based force spectroscopy shows a strong potassium-dependent interaction of WNV C with VLDL. When potassium buffer was replaced by sodium buffer, a dramatic decrease both in (un)binding events and rupture forces was observed, only unspecific interactions remaining. AFM-based force spectroscopy also shows that the WNV C interactions with LDL are weak and unspecific: an average rupture force of 24.53 pN was recorded, as well as a percentage of (un)binding events of 3.1%. All AFM data collected are in agreements with the data obtained by DLS.

As discussed in the background, LDL are originated from VLDL and present small but important differences. To become LDL, VLDL lose triacylglycerols and get enriched in cholesterol esters, become smaller in size and, additionally, they lose some of the VLDL intrinsic proteins. At the final stage, apoB100 is the most important apolipoprotein in the mature LDL and apoE is not present at their surface. apoE has some degree of similarity with LDs surface protein perilipin 3 or TIP47 (Faustino *et al*., 2014; Hickenbottom *et al.*, 2004). Considering that it was reported that DENV C interaction with LDs and VLDL occur through the binding to TIP47 (Carvalho *et al*., 2012) and apoE (Faustino *et al*., 2014), respectively, and that in the previous chapter we showed that WNV C can interact with LDs, it may be expected that WNV C-VLDL interaction also occur via apoE. Attending to this and the similarities between VLDL and LDs, the WNV C interaction may occur through a similar K^+-dependent mechanism, with the involvement of the WNV C N-terminal and the α2-α2' hydrophobic regions.

Regarding the interaction between WNV C and VLDL, the results obtained are consistent with the formation of a layer of WNV C dimer bound to the VLDL surface. The WNV C-VLDL complex radius increases ~2.3 nm, correlating very well with the size of WNV C. These findings lead to the hypothesis that WNV C may form LVPs. Probably WNV share this property with other *Flaviviridae*, such as HCV (Bartenschlager *et al.*, 2011), HGV and BVDV (Agnello *et al*., 1999), which enter host cells through the LDLR pathway (Agnello *et al.*, 1999). In agreement with this hypothesis, it is known that plasma lipoproteins levels in circulation are greatly affected in *Flavivirus* infections (Survana and

Rane, 2009; Bartenschlager *et al.*, 2011; van Grop *et al.*, 2002), in particular in the most severe cases of dengue infection, for which formation of LVPs had been hypothesized (Faustino *et al*., 2014). The formation of highly infectious WNV LVPs particles, via WNV C association with VLDL, may be an importantly process in WNV infection, eventually explaining its capacity to evade the host immune system and cross the BBB, causing systemic and neurologic diseases.

Through the observation of the autocorrelations functions of DLS measurements, it was possible to observe that pep14-23 can cause some inhibition of WNV C interaction with VLDL. VLDL alone presents an autocorrelation function decay identical to the observed in previous studies (Faustino *et al.*, 2014). In the presence of WNV C, VLDL present a slower autocorrelation function decay, due to the formation of complexes (WNV C binding do VLDL). This slower decay was also observed for VLDL in the presence of DENV C (Faustino *et al.*, 2014). When VLDL were previously incubated with pep14-23 and then titrated with WNV C, the autocorrelation functions decay is slower than for VLDL alone, but faster than for VLDL with WNV C in the absence of pep14-23. Despite the need of additional studies, pep14-23 seems to be a potential inhibitor of the interaction of WNV C with VLDL. In previous studies, it was reported that this peptide, designed based on the N-terminal of DENV C, can inhibit DENV C interaction with LDs (Martins *et al*., 2012), as well with VLDL (Faustino *et al.*, 2014). No treatment is available for WNV and DENV infections. Considering that DENV C and WNV C interaction occurs through surface proteins of VLDL and LDs (apoE and TIP47, respectively), and these proteins are similar in sequence and structure, it is possible that pep14-23 can also inhibit the interaction of WNV C with LDs and VLDL.

V - General Conclusions

The study was initiated with an analysis of WNV C interaction with LDs isolated from BHK-21 cells, employing zeta potential measurement. These results show that WNV C interact with LDs, exposing its α4-α4' region to the aqueous environment, and that this interactions is dependent on potassium ions. This potassium dependence of the interaction makes sense in the way that the potassium concentration is around 110 mM within the intracellular medium (Nelson and Cox, 2005), where this interaction is deemed to occur. Moreover, proteins from other viruses are known to have potassium-dependent functions, pointing out the importance that this ion may have for the viral life cycle progression. Zeta potential measurement with LDs preincubated with trypsin indicated that WNV C binding to LDs is also dependent of LDs surface proteins. In agreement with zeta potential results, AFM-based force spectroscopy measurements showed a strong and specific WNV C-LDs interaction dependent on the potassium ion. All data suggest a mechanism of WNV C interaction with LDs similar to what was described for the DENV C-LDs interaction. Generally, host lipid metabolism is strongly affected during *Flaviviridae* infections (Survana and Rane, 2009). This is a key process for the *Flaviviridae* life cycle to proceed (Boulant *et al.*, 2007; Samsa *et al.*, 2009). DENV and HCV capsid proteins interaction with LDs was found crucial for viral replication, maturation and assembly (Boulant *et al.*, 2007; Samsa *et al.*, 2009; Shavinskaya *et al.*, 2007). With the findings achieved in this study for WNV, we can conclude that the interaction of *Flaviviridae* C proteins with these intracellular organelles may be a key step of the life cycle conserved among these viruses.

In this study, WNV C was also found to interact with human VLDL. AFM-based force microscopy showed that this interaction is specific and also dependent on potassium ions. As the WNV C-VLDL interaction potassium dependence also was observed in the case of the interaction with LDs, this suggests a similar mechanism of binding between WNV C and these two lipid systems. Additionally, DLS measurements show that WNV C interacts with VLDL but not with LDL. The increase in the average diameter of VLDL observed upon the addition of WNV C perfectly correlated with WNV C dimensions. WNV had not been previously reported to form LVPs. However, the findings achieved in this study suggest that WNV C binds to VLDL and may form LVPs, entering in the cells via the LDLR pathway. In fact, formation of LVPs was previous described for other *Flavivirus* (Bartenschlager *et al.*, 2011). Recently in the host lab it was proposed that DENV C also interact with VLDL to form LVPs (Faustino *et al.*, 2014).

Considering that WNV C targets in LDs and VLDL are proteins, they should be either one that is found in both lipid systems, or different proteins with analogous structure or sequence, therefore providing similar binding sites. This is the case of TIP47 (perilipin 3) and apoE, proteins presents at the surface of LDs and VLDL, respectively. LDs and VLDL are similar in composition, but they have different functions and do not share the same proteins. However, apoE has a remarkable structural and sequence similarity with TIP47, pointing them as possible targets for WNV C binding. In the current model for WNV C function, the α2-α2' would interact with lipids and the α4-α4' region with the viral RNA (Ma *et al.*, 2004). It is important to consider that proteins found on LDs and structurally analogous proteins found in VLDL also have a specific role in the interaction with the capsid protein.

With this knowledge, we also performed DLS measurements to test the ability of pep14-23, an inhibitor of DENV C interaction with LDs and with VLDL, to inhibit the interaction of WNV C with VLDL. The results suggest that the peptide may be an inhibitor of WNV C interaction with lipid systems; however, more studies have to be performed to understand their potentiality. pep14-23 was designed based on the N-terminal region of DENV C. The peptide contains a conserved sequence and some more residues, not conserved but found to be important for the DENV C-LDs interaction; thus, it can be expected that pep14-23 is an effective inhibitor against *Flavivirus* interaction with lipid systems.

Future Work

The results described in this work indicate that WNV C binds to LDs and VLDL. In addition, the host lab previously showed that DENV C also interacts with VLDL, which may ultimately lead to the formation of highly infectious lipoviroparticles. The LDs surface proteins responsible for the binding were also determined. Considering that DENV and WNV C proteins are very similar in terms of structure and sequence, and that the specific residues of the DENV C responsible for its interaction with LDs (a process essential for viral replication) were identified, similar mechanisms may occur in WNV and, thus, a similar rationale may now be applied to the inhibition of WNV infection. DLS measurements with pep14-23, an inhibitor of DENV C interaction with LDs, therefore potentially impairing viral replication, shows that this peptide may inhibit the interaction of WNV C with VLDL. In future work, AFM-based force spectroscopy measurements to quantify at the single-molecule level WNV C binding to LDs and lipoproteins, in the presence and absence of rationally designed inhibitor peptides will be performed to understand the ability of the peptide to inhibit the interaction of WNV C with LDs and VLDL. These findings will be important to understand if pep14-23 is a potential inhibitor of *Flavivirus* viral replication. In a second step, viral replication inhibition assays in kidney cell lines will determine if pep14-23 is efficient. Computational analysis of protein-ligand interactions will also be performed to establish the specific details of WNV C interaction with lipid droplets and lipoproteins. These findings may allow the development of inhibitors of the capsid protein-mediated mechanism of WNV assembly, and the development of therapeutic approaches with a possible applicability to other flaviviruses.

References

Agnello, V., Abel, G., Elfahal, M., Knight, G.B. e Zhang, Q.X. 1999. Hepatitis C virus and other flaviviridae viruses enter cells via low density lipoprotein receptor. Proc Natl Acad Sci USA. 96: 12766-12771.

André, P., Komurian-Pradel, F., Deforges, S., Perret, M., Berland, J.L., Sodoyer, M., Pol, S., Bréchot, C., Paranhos-Baccalà, G. e Lotteau, V. 2002. Characterization of low- and very low-density hepatitis C virus RNA-containing particles. J Virol. 76: 6919-6928.

Assunção-Miranda, I., Bozza, M.T. e Da Poian, A.T. 2010. Pro-inflammatory response resulting from sindbis virus infection of human macrophages: implications for the pathogenesis of viral arthritis. J Med Virol. 82: 164-174.

Bagnarelli, P., Marinelli, K., Trotta, D., Monachetti, A., Tavio, M., Del Gobbo, R., Capobianchi, M., Menzo, S., Nicoletti, L., Magurano, F. e Varaldo, P. 2011. Human case of autochthonous West Nile virus lineage 2 infection in Italy. Euro Surveill.16 pii: 20002.

Barba, G., Harper, F., Harada, T., Kohara, M., Goulinet, S., Matsuura, Y., Eder, G., Schaff, Z., Chapman, M.J., Miyamura, T. e Bréchot, C. 1997. Hepatitis C virus core protein shows a cytoplasmic localization and associates to cellular lipid storage droplets. Proc Natl Acad Sci USA. 94: 1200-1205.

Barros, S.C., Ramos, F., Fagulha, T., Duarte, M., Henriques, M., Luis, T. e Fevereiro, M. 2011. Serological evidence of West Nile virus circulation in Portugal. Vet Microbiol. 152: 407-410.

Bartenschlager, R., Penin, F., Lohmann, V. e André, P. 2011. Assembly of infectious hepatitis C virus particles. Trends Microbiol. 19: 95-103.

Berne, B.J. e Pecora, R. 1990. Dynamic Light Scattering – With Application to Chemistry. In Biology and Physics (Robert E ed), pp. 4-23, Krieger Publishing Company, Melbourne, Australia.

Bhuvanakantham, R. e Ng, M.L. 2013. West Nile virus and dengue virus capsid protein negates the antiviral activity of human Sec3 protein through the proteasome pathway. Cell Microbiol. 15: 1688-1706.

Bhuvanakantham, R., Chong, M.K. e Ng, M.L. 2009. Specific interaction of capsid protein and importin-alpha/beta influences West Nile virus production. Biochem Biophys Res Commun. 389: 63-69.

Bhuvanakantham, R., Li, J., Tan, T.T. e Ng, M.L. 2010 Human Sec3 protein is a novel transcriptional and translational repressor of flavivirus. Cell Microbiol. 12: 453-472.

Boulant, S., Targett-Adams, P. e McLauchlan, J. 2007. Disrupting the association of hepatitis C virus core protein with lipid droplets correlates with a loss in production of infectious virus. J Gen Virol. 88: 2204-2213.

Bowen, G.S., Monath, T.P., Kemp, G.E., Kerschner, J.H. e Kirk, L.J. 1980. Geographic variation among St. Louis encephalitis virus strains in the viremic responses of avian hosts. Am J Trop Med Hyg. 29: 1411-1419.

Brinton, M.A. 2013. Replication cycle and molecular biology of the West Nile virus. Viruses. 6: 13-53.

Busch, M.P., Kleinman, S.H., Tobler, L.H., Kamel, H.T., Norris, P.J., Walsh, I., Matud, J.L., Prince, H.E., Lanciotti, R.S., Wright, D.J., Linnen, J.M. e Caglioti, S. 2008. Virus and antibody dynamics in acute west nile virus infection. J Infect Dis. 198: 984-993.

Campbell, G.L., Marfin, A.A., Lanciotti, R.S. e Gubler, D.J. 2002. West Nile virus. Lancet Infect. Dis. 2: 519-529.

Carvalho, F.A. e Santos, N.C. 2012. Atomic force microscopy-based force spectroscopy--biological and biomedical applications. IUBMB Life. 64: 465-472.

Carvalho, F.A., Carneiro, F.A., Martins, I.C., Assuncao-Miranda, I., Faustino, A.F., Pereira, R.M., Bozza, P.T., Castanho, M.A., Mohana-Borges, R., Da Poian, A.T. e Santos, N.C. 2012. Dengue virus capsid protein binding to hepatic lipid droplets (LD) is potassium ion dependent and is mediated by LD surface proteins. J Virol. 86: 2096-2108.

Ciota, A,T. e Kramer, L.D. 2013. Vector-virus interactions and transmission dynamics of West Nile virus. Viruses. 5: 3021-3047.

Civen, R., Villacorte, F., Robles, D.T., Dassey, D.E., Croker, C., Borenstein, L., Harvey, S.M. e Mascola, L. 2006. West Nile Virus Infection in the Pediatric Population. Pediatr Infect Dis J. 25: 75-78.

Counihan, N.A., Rawlinson, S.M. e Lindenbach, B.D. 2011. Trafficking of hepatitis C virus core protein during virus particle assembly. PLoS Pathog. 7:e1002302.

Cushley, R.J. e Okon, M. 2002. NMR studies of lipoprotein structure. Annu Rev Biophys Biomol Struct. 31: 177-206.

Desmeules, P., Grandbois, M., Bondarenko, V.A., Yamazaki, A. e Salesse, C. 2002. Measurement of membrane binding between recoverin, a calcium-myristoyl switch protein, and lipid bilayers by AFM-based force spectroscopy. Biophys J. 82: 3343-3350.

Diamond, M.S. 2009. Progress on the development of therapeutics against West Nile virus. Antiviral Res. 83: 214-227.

Ding, Y., Zhang, S., Yang, L., Na, H., Zhang, P., Zhang, H., Wang, Y., Chen, Y., Yu, J., Huo, C., Xu, S., Garaiova, M., Cong, Y. e Liu, P. 2013. Isolating lipid droplets from multiple species. Nat Protoc. 8: 43-51.

Dokland, T., Walsh, M., Mackenzie, J.M., Khromykh, A.A., Ee, K.H. e Wang, S. 2004. West Nile virus core protein: tetramer structure and ribbon formation. Structure. 12: 1157-1163.

Domingues, M.M., Santiago, P.S., Castanho, M.A. e Santos, N.C. 2008. What can light scattering spectroscopy do for membrane-active peptide studies? J Pept Sci. 14: 394-400.

Faustino, A.F., Carvalho, F.A., Martins, I.C., Castanho, M.A., Mohana- Borges, R., Da Poian, A.T. e Santos, N.C. 2014. Dengue Virus Capsid Protein Interacts Specifically with Very Low Density Lipoproteins. Nanomedicine. 10: 247-255.

Granwehr, B.P., Lillibridge, K.M., Higgs, S., Mason, P.W., Aronson, J.F., Campbell, G.A. e Barrett, A.D. 2004. West Nile virus: Where are we now? Lancet Infect Dis. 4: 547-556.

Gray, T.J. e Webb, C.E. 2014. A review of the epidemiological and clinical aspects of West Nile virus. Int J Gen Med. 11: 193-203.

Griffin, S.D., Beales, L.P., Clarke, D.S., Worsfold, O., Evans, S.D., Jaeger, J., Harris, M.P. e Rowlands, D.J. 2003. The p7 protein of hepatitis C virus forms an ion channel that is blocked by the antiviral drug, Amantadine. FEBS Lett. 535: 34-38.

Heaton, N.S., Perera, R., Berger, K.L., Khadka, S., Lacount, D.J., Kuhn, R.J. e Randall, G. 2010. Dengue virus nonstructural protein 3 redistributes fatty acid synthase to sites of viral replication and increases cellular fatty acid synthesis. Proc Natl Acad Sci USA. 40: 17345-17350.

Hickenbottom, S.J., Kimmel, A.R., Londos, C. e Hurley, J.H. 2004. Structure of a lipid droplet protein; the PAT family member TIP47. Structure. 12: 1199-1207.

Hinterwirth, H., Wiedmer, S.K., Moilanen, M., Lehner, A., Allmaier, G. e Waitz, T., Lindner, W., Lämmerhofer, M. 2013. Comparative method evaluation for size and size-distribution analysis of gold nanoparticles. J Sep Sci. 36: 2952-2961.

Hussmann, K.L., Vandergaast, R.L., Zheng, K., Hoover, L.I. e Fredericksen, B.L. 2014. Structural proteins of West Nile virus are a major determinant of infectious particle production and fitness in astrocytes. J Gen Virol. 95: 1991-2003.

Ivanyi-Nagy, R. e Darlix, J.L. 2010. Intrinsic disorder in the core proteins of flaviviruses. Prot Pept Lett. 17: 1019-1025.

Ivanyi-Nagy, R., Lavergne, J.P., Gabus, C., Ficheux, D. e Darlix, J.L. 2008. RNA chaperoning and intrinsic disorder in the core proteins of Flaviviridae. Nucleic Acids Res. 36: 712-725.

Johnston, L.J., Halliday, G.M. e King, N.J. 2000. Langerhans cells migrate to local lymph nodes following cutaneous infection with an arbovirus. Invest Dermatol. 114: 560-568.

Jones, C.T., Ma, L., Burgner, J.W., Groesch, T.D., Post, C.B. e Kuhn, R.J. 2003. Flavivirus capsid is a dimeric alpha-helical protein. J Virol. 77: 7143-7149.

Kilpatrick, A.M. 2011. Globalization, land use, and the invasion of West Nile virus. Science. 334: 323-327.

Kimura, T., Sasaki, M., Okumura, M., Kim, E. e Sawa, H. 2010. Flavivirus encephalitis: pathological aspects of mouse and other animal models. Vet Pathol. 47: 806-818.

Kirby, B. e Hasselbrink, E. 2004. Zeta potential of microfluidic substrates: 1. Theory, experimental techniques, and effects on separations. Electrophoresis 25: 187-202.

Krahmer, N., Farese, R.V. Jr. e Walther, T.C. 2013. Balancing the fat: lipid droplets and human disease. EMBO Mol Med. 5: 905-915.

Krahmer, N., Guo, Y., Farese, R.V. Jr. e Walther, T.C. 2009. SnapShot: Lipid Droplets. Cell. 139: 1024-1024.

Lim, P.Y., Behr, M.J., Chadwick, C.M., Shi, P.Y. e Bernard, K.A. 2011. Keratinocytes are cell targets of West Nile virus in vivo. J Virol. 85: 5197-5201.

Lim, S.M., Koraka, P., Osterhaus, A.D. e Martina, B.E. 2011. West Nile virus: immunity and pathogenesis. Viruses. 3: 811-828.

Lin, P., Chen, X., Moktan, H., Arrese, E.L., Duan, L., Wang, L., Soulages, J.L. e Zhou, D.H. 2014. Membrane attachment and structure models of lipid storage droplet protein 1. Biochim Biophys Acta.1838: 874-881.

Lindsey, N.P., Hayes, E.B., Staples, J.E. e Fischer, M. 2009. West Nile virus disease in children, United States, 1999–2007. Pediatrics. 123: 1084-1089.

Ma, L., Jones, C.T., Groesch, T.D., Kuhn, R.J. e Post, C.B. 2004. Solution structure of dengue virus capsid protein reveals another fold. Proc Natl Acad Sci USA. 101: 3414-3419.

Mankouri, J., Dallas, M.L., Hughes, M.E., Griffin, S.D., Macdonald, A. e Peers, C., Harris, M. 2009. Suppression of a pro-apoptotic K+ channel as a mechanism for hepatitis C virus persistence. Proc Natl Acad Sci USA. 106: 15903-15908.

Martins, I.C., Gomes-Neto, F., Faustino, A.F., Carvalho, F.A., Carneiro, F.A., Bozza, P.T., Mohana-Borges, R., Castanho, M.A., Almeida, F.C., Santos, N.C. e Da Poian, A.T. 2012. The disordered N-terminal region of dengue virus capsid protein contains a lipid droplet-binding motif. Biochem J. 444: 405-415.

McLauchlan, J. 2000. Properties of the hepatitis C virus core protein: a structural protein that modulates cellular processes. J Viral Hepat. 7: 2-14.

McLauchlan, J. 2009. Hepatitis C virus: viral proteins on the move. Biochem Soc Trans. 37: 986-990.

Miller, J.F., Schatzel, K. e Vincent, B. 1991. The determination of very small electrophoretic mobilities in polar and nonpolar colloidal dispersions using phase-analysis light-scattering. J Colloid Interface Sci. 143: 532-554.

Miller, S. e Krijnse-Locker, J. 2008. Modification of intracellular membrane structures for virus replication. Nat Rev Microbiol. 6: 363-374.

Mukhopadhyay, S., Kim, B.S., Chipman, P.R., Rossmann, M.G. e Kuhn, R.J. 2003. Structure of West Nile virus. Science. 302:248.

Mukhopadhyay, S., Kuhn, R.J. e Rossmann, M.G. 2005. A structural perspective of the flavivirus life cycle. Nat Rev Microbiol. 3: 13-22.

Murray, K.O., Garcia, M.N., Yan, C. e Gorchakov, R. 2013. Persistence of detectable immunoglobulin M antibodies up to 8 years after infection with West Nile virus. Am J Trop Med Hyg. 89: 996-1000.

Nelson, D.L. e Cox, M.M. 2005. Lehninger Principles of Biochemistry. Ed. W.H.Freeman & Co Ltd.

Netsawang, J., Noisakran, S., Puttikhunt, C., Kasinrerk, W., Wongwiwat, W., Malasit, P., Yenchitsomanus, P.T. e Limjindaporn, T. 2010. Nuclear localization of dengue virus capsid protein is required for DAXX interaction and apoptosis. Virus Res. 147: 275-283.

O'Leary, D.R., Marfin, A.A., Montgomery, S.P., Kipp, A.M., Lehman, J.A., Biggerstaff, B.J., Elko, V.L., Collins, P.D., Jones, J.E. e Campbell, G.L. 2004. The epidemic of West Nile virus in the United States, 2002. Vector Borne Zoonotic Dis. 4: 61-70.

Olofsson, S.O., Boström, P., Andersson, L., Rutberg, M., Perman, J. e Borén, J. 2009. Lipid droplets as dynamic organelles connecting storage and efflux of lipids. Biochim Biophys Acta. 1791: 448-458.

Papa, A., Danis, K., Athanasiadou, A., Delianidou, M. e Panagiotopoulos, T. 2011. Persistence of West Nile virus immunoglobulin M antibodies, Greece. J Med Virol. 83: 1857-1860.

Pauli, G., Bauerfeind, U., Blümel, J., Burger, R., Drosten, C., Gröner, A., Gürtler, L., Heiden, M., Hildebrandt, M., Jansen, B., Montag-Lessing, T., Offergeld, R., Seitz, R.,Schlenkrich, U., Schottstedt, V., Strobel, J. e Willkommen H. 2013. West nile virus. Transfus Med Hemother. 40: 265-284.

Pol, A., Gross, S.P. e Parton, R.G. 2014. Review: biogenesis of the multifunctional lipid droplet: lipids, proteins, and sites. J Cell Biol. 204: 635-646.

Ratto, T.V., Rudd, R.E., Langry, K.C., Balhorn, R.L. e McElfresh, M.W. 2006. Nonlinearly additive forces in multivalent ligand binding to a single protein revealed with force spectroscopy. Langmuir 22: 1749-1757.

Reisen, W.K. 2010. Landscape epidemiology of vector-borne diseases. Annu Rev Entomol. 55: 461-483.

Reiter, P. 2010. West Nile virus in Europe: understanding the present to gauge the future. Euro Surveill. 15: 19508.

Rossi, S.L., Ross, T.M. e Evans, J.D. 2010. West Nile virus. Clin Lab Med. 30: 47-65.

Saiyasombat, R., Carrillo-Tripp, J., Miller, W.A., Bredenbeek, P.J. e Blitvich, B.J. 2014. Substitution of the premembrane and envelope protein genes of Modoc virus with the homologous sequences of West Nile virus generates a chimeric virus that replicates in vertebrate but not mosquito cells. Virol J. 11: 150.

Samsa, M.M., Mondotte, J.A., Iglesias, N.G., Assuncao-Miranda, I., Barbosa-Lima, G., Da Poian, A.T., Bozza, P.T. e Gamarnik, A.V. 2009. Dengue virus capsid protein usurps lipid droplets for viral particle formation. PLoS Pathog. 5: e1000632.

Samuel, M.A. e Diamond, M.S. 2005. Alpha/beta interferon protects against lethal West Nile virus infection by restricting cellular tropism and enhancing neuronal survival. J Virol. 79: 13350-13361.

Santos, N.C. e Castanho, M.A. 1996. Teaching light scattering spectroscopy: the dimension and shape of tobacco mosaic virus. Biophys J. 71: 1641-1650.

Santos, N.C. e Castanho, M.A. 2004. An overview of the biophysical applications of atomic force microscopy. Biophys Chem. 107: 133-149.

Sejvar, J.J. 2014. Clinical Manifestations and Outcomes of West Nile Virus Infection. Viruses. 6: 606-623.

Shavinskaya, A., Boulant, S., Penin, F., McLauchlan, J. e Bartenschlager R. 2007. The lipid droplet binding domain of hepatitis C virus core protein is a major determinant for efficient virus assembly. J Biol Chem. 282: 37158-37169.

Suvarna, J.C. e Rane, P.P. 2009. Serum lipid profile: a predictor of clinical outcome in dengue infection. Trop Med Int Health. 14: 576-585.

Tesh, R.B., Siirin, M., Guzman, H., Travassos da Rosa, A.P., Wu, X., Duan, T., Lei, H., Nunes, M.R. e Xiao, S.Y. 2005. Persistent West Nile virus infection in the golden hamster: studies on its mechanism and possible implications for other flavivirus infections. J Infect Dis. 192: 287-295.

Thiam, A.R., Farese, R.V, Jr. e Walther, T.C. 2013. The biophysics and cell biology of lipid droplets. Nat Rev Mol Cell Biol. 14: 775-786.

Urcuqui-Inchima, S., Patiño, C., Torres, S., Haenni, A.L. e Díaz, F.J. 2010. Recent developments in understanding dengue virus replication. Adv Virus Res. 77: 1-39.

Uskoković, V. 2012. Dynamic Light Scattering Based Microelectrophoresis: Main Prospects and Limitations. J Dispers Sci Technol. 33: 1762-1786.

Vahabi, S., Nazemi Salman, B. e Javanmard, A. 2013. Atomic force microscopy application in biological research: a review study. Iran J Med Sci. 38: 76-83.

van Gorp, E.C., Suharti, C., Mairuhu, A.T., Dolmans, W.M., van Der Ven, J., Demacker, P.N. e van Der Meer, J.W. 2002. Changes in the plasma lipid profile as a potential predictor of clinical outcome in dengue hemorrhagic fever. Clin Infect Dis. 34: 1150-1153.

Vogt, D.A., Camus, G., Herker, E., Webster, B.R., Tsou, C.L., Greene, W.C., Yen, T.S. e Ott, M. 2013. Nat Rev Mol Cell Biol. 14: 775-786. Lipid droplet binding protein TIP47 regulates hepatitis C Virus RNA replication through interaction with the viralNS5A protein. PLoS Pathog. 9:e1003302.

Walther, T.C. e Farese, R.V. Jr. 2009. The life of lipid droplets. Biochim Biophys Acta. 1791: 459-466.

Wang, K., Xie, S. e Sun, B. 2011. Viral proteins function as ion channels. Biochim Biophys Acta. 1808: 510-515.

Whited, A.M. e Park, P.S. 2014. Atomic force microscopy: multifaceted tool to study membrane proteins and their interactions with ligands. 1838: 56-68.

Willemsen, O.H., Snel, M.M., Cambi, A., Greve, J., De Grooth, B.G. e Figdor, C.G. 2000. Biomolecular interactions measured by atomic force microscopy. Biophys J. 79: 3267-3281.

Wilson, C.A. e Bale, J.F. Jr. 2014. West nile virus infections in children. Curr Infect Dis Rep. 16: 391.

Yang, S.C., Paik, S.Y., Ryu, J., Choi, K.O., Kang, T.S., Lee, J.K., Song, C.W. e Ko, S. 2014. Dynamic light scattering based method to determine primary particle size of iron oxide nanoparticles in simulatedgastrointestinal fluid. Food Chem. 161: 185-191.

Yu, I.M., Zhang, W., Holdaway, H.A. e Li, L., Kostyuchenko, V.A., Chipman, P.R., Kuhn, R.J., Rossmann, M.G., Chen, J. 2008. Structure of the immature dengue virus at low pH primes proteolytic maturation. Science. 319: 1834-1837.

Annexes

Annex 1

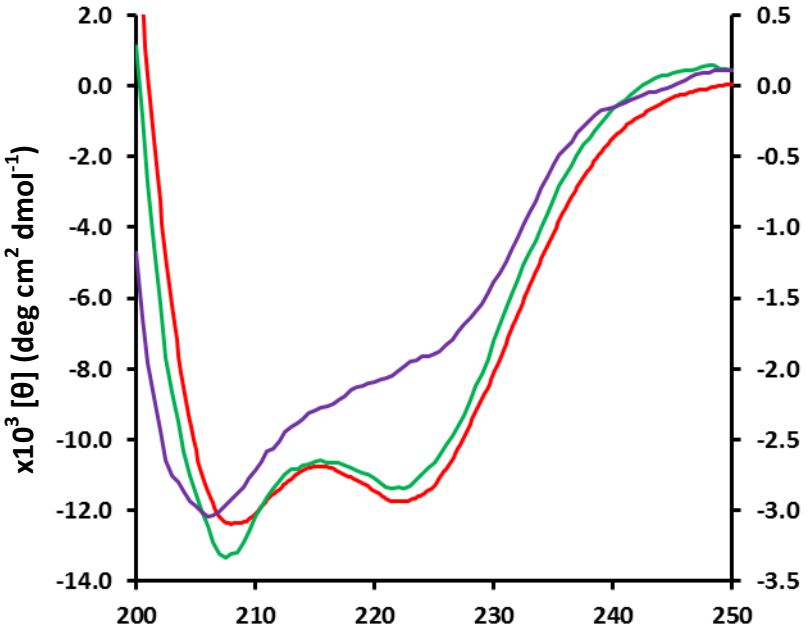

Supplementary Figure 1 - CD spectra of the recombinant DENV C, synthetic DENV C and synthetic WNV C. The CD spectra of recombinant DENV C (red) and synthetic DENV C (green), represented in the left y axis, are very identical and rich in α-helical structure. The CD spectra of synthetic WNV C (purple), represented in the right y axis, presents random coil content as well as α-helix motifs.

Annex 2

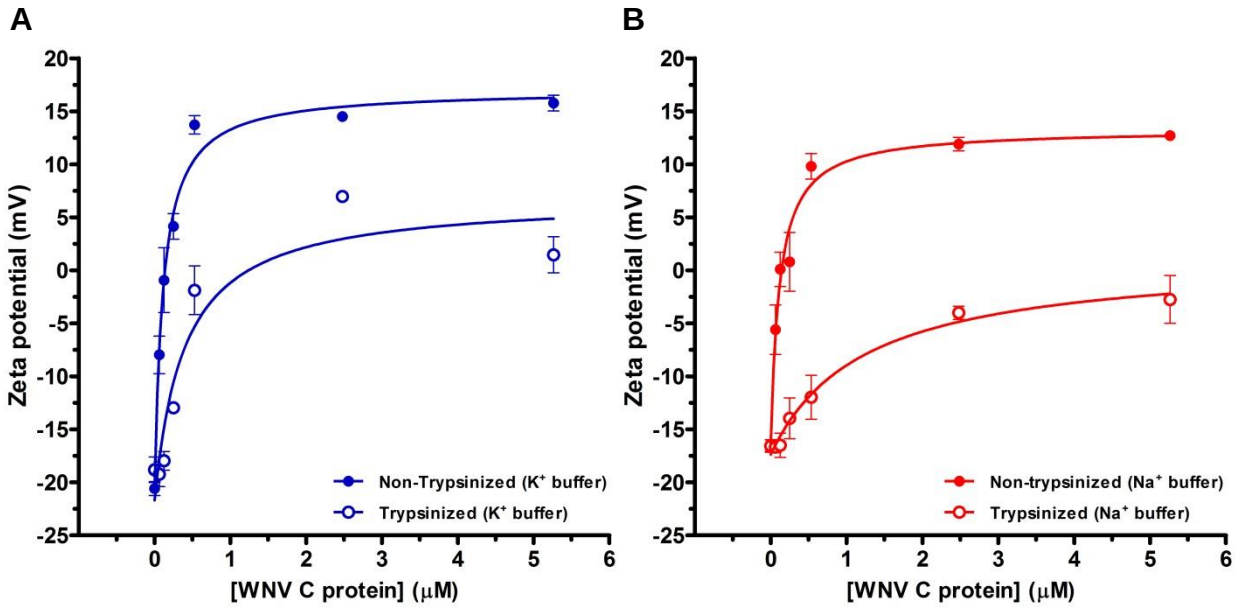

Supplementary Figure 2 - Zeta potential values of LDs samples isolated in (A) TEE-KCl buffer or (B) TEE-NaCl buffer, in the absence and in the presence of distinct WNV C concentrations. Zeta potential values were determined for LDs without trypsin treatment (filled symbols) and LDs preincubated with trypsin (empty symbols). The values are represented as mean ± standard error, and solid lines were obtained by fitting the experimental data with equation 10.